Wheel Speed Sensor Signal Processing for Tyre-Road Friction Estimation

Master Thesis
DC 2016.070

Manikandan Manjaparai Sundaram-0926898
Master's in Automotive Technology

Supervisors : dr. ir. A. J. C. Schmeitz[1] (External Supervisor)
dr. ir. I. J. M. Besselink[2] (Internal Supervisor)

Graduation Professor: Prof. dr. H. Nijmeijer[2]

[1] TNO Automotive
Integrated Vehicle Safety Department
Helmond

[2] Eindhoven University of Technology (TU/e)
Department of Mechanical Engineering
Dynamics and Control Group
Eindhoven

September 2016

TU/e Technische Universiteit Eindhoven University of Technology

Declaration concerning the TU/e Code of Scientific Conduct

I have read the TU/e Code of Scientific Conduct[i].

In carrying out research, design and educational activities, I shall observe the five central values of scientific integrity, namely: trustworthiness, intellectual honesty, openness, independence and societal responsibility, as well as the norms and principles which follow from them.

Date

14/09/2016

Name

MANIKANDAN MANIAPARAI SUNDARAM

ID-number

0926898

Signature

Submit the signed declaration to the student administration of your department.

[i] See: http://www.tue.nl/en/university/about-the-university/integrity/scientific-integrity/
The Netherlands Code of Conduct for Academic Practice of the VSNU can be found here also.
More information about scientific integrity is published on the websites of TU/e and VSNU

January 15 2016

Abstract

The prediction of tyre-road friction plays a crucial role in many vehicle active safety systems. One of the interesting approaches to estimate the tyre-road friction for a normal driving condition is by monitoring the first tyre resonance frequency from the wheel speed signal. The first tyre resonance frequency is used as an indication for friction, i.e. the damping ratio of the first tyre resonance frequency decreases with the increase in tyre-road friction. However, the performance of the friction estimation primarily depends on the processing of the wheel speed signal. This processing includes converting the event based wheel speed data from the ABS wheel speed sensor to a time based wheel speed signal.

The ABS wheel speed sensor uses an event based sampling approach, i.e the signal is sampled only when a pre-defined event occurs. The wheel speed sensor unit consists of a toothed wheel and an inductive sensor such that the information from the sensor unit is received only when the toothed edge passes the inductive sensor. However, the toothed wheel is not ideal and is subjected to periodic pulse width errors. These pulse width errors occur at each edge of the sensor toothed wheel and are caused by mechanical tolerances during the production. Further, these pulse width errors reduces the quality of the wheel speed signal when trying to identify the first tyre resonance frequency. In this thesis, a method to identify the pulse width errors in the event domain is developed. The developed method is based on a parameter identification algorithm to recursively estimate the pulse width errors for each edge of the sensor toothed wheel. Furthermore, in order to transform the event based to the time based signal, a suitable re-sampling method is proposed, such that the wheel speed signal is obtained with minimum aliasing effects. This is done to obtain a wheel speed signal with a fixed sample period for identifying the first tyre resonance frequency. The performance of the proposed methods are first evaluated in a simulation environment, which gives the possibility to compare the estimated pulse width errors with that of the modelled (artificial) pulse width errors. The developed methods are further assessed by tests using vehicle measurement data. It is concluded that the periodic pulse width errors can be estimated with reasonable accuracy and that the quality of the wheel speed signal after pulse width error compensation is greatly improved. The first tyre resonance is clearly observed from the corrected wheel speed signal, without any disturbances due to pulse width errors. Henceforth, the results from the developed wheel speed sensor processing give opportunities to identify the first tyre resonance frequency, and from this the friction of various road surfaces can be possibly estimated.

Nomenclature

Abbreviations

TPMS	Tyre Pressure Monitoring systems
ADAS	Advanced Driver Assistance Systems
ABS	Anti-lock Braking System
ESC	Electronic Stability Control
CAN	Controller Area Network
ATP	Automotive Testing Papenburg
RLS	Recursive Least Squares
LI	Linear Interpolation
PCHIP	Piecewise Cubic Hermite Interpolating Polynomial
IS	Integrated Sampling
PSD	Power Spectral Density
PWE	Pulse Width Errors
FL	Front Left
FR	Front Right
RL	Rear Left
RR	Rear Right

Subscripts

k	Detected edge
k-1	Previous edge
c	Computed
i	Instantaneous
r	Revolution

Symbols

Symbol	Description	Unit
$\Omega_{i,k}$	Instantaneous wheel speed at every detected edge	rad/s
$\Omega_{c,k}$	Computed wheel speed at every detected edge	rad/s
Ω_k	Corrected wheel speed at every detected edge	rad/s
Δt	Fixed sample period	s
d	Design parameter	-
t_k	Time instants at every detected edge	s
Δt_{clock}	Fixed clock sample period	s
α	Angle between last two detected edges	rad
N_{edge}	Number of edges detected by the sensor at each tooth	-
L	Total number of teeth in the sensor toothed wheel	-
δ_k	Pulse width errors at every detected edge	rad
f_{fund}	Fundamental frequency of the signal	Hz
Δt_k	Time period between last two detected edges	s
θ_k	Parameter to estimate	rad
$\hat{\theta}_k$	Estimated parameter	rad
J_k	Cost function	-
v_k	System noise	rad
λ	Forgetting factor	-
H_k	Input regression vector	-
ε_k	Estimation error	rad
P_k	Covariance matrix	-
K_k	Gain matrix	-
N	Total number of detected edges by the sensor	-
γ^{-1}	Regulation parameter	-
y_k	Measurement output	rad
p	Number of the sample with fixed sample period	-
f_k	Frequency of the edge detection	Hz
$\hat{\Omega}_k^0$	Reference wheel speed at every detected edge	rad/s
$\hat{\theta}_r$	Parameter estimate for all detected edges in one revolution	rad
y_r	Measurement output for all detected edges in one revolution	rad
H_r	Input regression matrix in one revolution	-
ε_r	Estimation error for all detected edges in one revolution	rad
m	Revolution counter	-
f_s	Sampling frequency	Hz
f_N	Nyquist frequency	Hz
R	Rolling radius of the tyre	m

Contents

Chapter 1

Introduction

The tyre-road friction coefficient is one of the most important parameters from the viewpoint of automotive safety. In this respect, several Advanced Driver Assistance Systems (ADAS) could benefit from knowing the friction potential, i.e. the maximum force that can be developed between road and tyre. In particular, having a reliable estimate of the friction coefficient for various road surfaces, will help automated vehicles to take necessary actions in order to improve the safety performance.

TNO has been developing technologies for ADAS for many years. As a result of increase in vehicle automation, importance of knowing the maximum possible tyre force or tyre road friction coefficient increases. Hence, it is highly necessary to estimate tyre-road friction in order to give conclusions on when the brake needs to be applied to prevent collision. Tyre road friction estimation is already available in many vehicle active safety systems like Anti-Lock Braking System (ABS) and Electronic Stability Control (ESC), however, the estimation algorithms require a large slip/acceleration to get a reliable estimate. Hence, the current challenge is to develop a tyre-road friction estimator working under normal driving conditions, i.e. in the low slip region, where no or low accelerations occur. TNO is planning to develop an integrated longitudinal friction estimator that combines several friction estimation algorithms and information obtained from several sensors. The algorithms are developed and evaluated using vehicle measurements.

1.1 Project background

An interesting method to estimate the tyre-road friction is using the first tyre resonance frequency, which can be seen in the wheel speed signal. This method is described using a tyre vibration model and an estimation algorithm, which can be found in various references [1], [2] and, [3]. The resonance frequency visible in the wheel speed signal is already used as an indirect way to measure the tyre inflation pressure, where the excitation of the vibration mode is caused by the road unevenness [4]. The observed phenomenon is that the first tyre resonance frequency reduces when the tyre pressure drops. In [5], it is described

that for a free rolling tyre of a vehicle, the first tyre resonance frequency is observed at 37 Hz when the tyre inflation pressure is around 200 kPa and decreased to 31 Hz when the tyre inflation pressure is reduced to 100 kPa.

In [1]and [2], a dynamic tyre model is used to estimate tyre-road friction from the first tyre resonance frequency seen in the wheel speed signal. The relation between damping ratio and natural frequency with longitudinal slip stiffness is used to estimate the friction. The assumption is that friction and slip stiffness are related. Further, using the tyre vibration model, a first tyre resonance peak around a frequency of 40 Hz is observed on a dry asphalt surface but the first tyre resonance is not observed on low friction surfaces. In addition to a tyre model, an instrumental variable (IV) estimation algorithm is used to estimate the resonance frequency and damping ratio of the first tyre resonance mode. Furthermore, it is shown that the developed friction estimation algorithm can detect friction changes from high to low and vice versa. According to the developed tyre model, the damping ratio obtained is inversely proportional to the longitudinal slip stiffness.

In [3], a detailed vehicle model, including the MF-Swift tyre model, is presented to investigate the behaviour of the simulated wheel speed signal, which includes the first tyre resonance frequency. Apart from the wheel speed signal, the damping ratio and the resonance frequency of the tyre are also obtained from the model. When the natural frequency and damping ratio are evaluated using the model, it appears that these do not satisfy the simple tyre vibration model used in [1]. The damping ratio indeed increases with a decrease in longitudinal slip stiffness, however the damping ratios are not inversely proportional to the longitudinal slip stiffness as indicated by [1]. This suggests that the simple tyre model in [1] is not accurate enough to estimate the longitudinal slip stiffness from the identified damping ratio and natural frequency. In addition to the MF-Swift tyre model, the estimation algorithm used in [1] is also implemented in [3] and applied to simulated wheel speeds. This is in order to compare the estimated resonance frequency and damping ratio values with the known values obtained from the simulation model. The frequency content of the wheel speed signal show that the first tyre resonance occurs around 35 Hz [3]. In [3], it is concluded that the estimated damping ratio and resonance frequency are reasonably accurate and hence the damping of the resonance frequency is a measure for friction.

In the summer of 2015, test data had been gathered by TNO for different road conditions, i.e. for both high friction and low friction surfaces. So far, the friction estimation method was validated using a simulation environment, and not using the test data. This is due to some issues with processing of the wheel speed data [6], i.e. the frequency content of the wheel speed signals from the test data do not correspond with those obtained with the simulation model in [3] and also not with measurement results from [1].

Normally, the wheel speed signals are available on the Controller Area Network (CAN) bus. Between the sensor unit and the CAN bus, a signal processing black box is present, which performs the sampling and filtering of the raw data. Thus, the wheel speeds from the

CAN bus are black-box processed and do not contain the required high frequency content as the data is affected by filtering. Therefore, a clear first tyre resonance frequency peak in wheel speed signal is hard to identify. To solve this issue, TNO uses a separate dSPACE auto box, which stores the raw data from the sensors and can replace the signal processing black box. The processing method of the wheel speed data can be freely designed in order to check whether it is possible to identify the first tyre resonance frequency from the wheel speed signal.

In [6], a theoretical background on the processing of a wheel speed signal is given, however, the actual implementation is not made. The part on how the resonance method is applied to estimate friction is studied, implemented, and compared with the CAN data. Since processing of the wheel speed signal is insufficient, the method developed does not give a good estimate of the friction. This is the major reason for developing a suitable processing method in order to identify a clear first tyre resonance frequency.

The default CAN wheel speed sensor processing usually involves sampling and low pass filtering of the data. The primary motivation of this thesis is to obtain the first tyre resonance frequency, without filtering it out as in the case with the existing black box algorithms. Further, the quality of the wheel speed signals from the ABS wheel speed sensors are not accurate, as these are affected by periodic Pulse Width Errors (PWE) due to irregularities in the sensor toothed wheel. These PWE are assumed to be a dominating disturbance in the wheel speed signals. The irregularities are mainly due to mechanical tolerances during the production of the sensor toothed wheel. Another challenge in the processing of the wheel speed sensor data is that the ABS wheel speed sensor are event based sampled and the raw data is received as series of events. Hence, a suitable method has to be developed in order to correct the pulse width errors in the event domain and convert the corrected wheel speed data to the time domain.

1.2 Problem definition

The main objective of this research work is "To develop a suitable method to process the event based wheel speed data from the ABS wheel speed sensor such that a sampled time domain signal is available, containing sufficient high frequency content for estimating the first tyre resonance frequency and damping ratio".

To reach this objective, the following areas should be investigated:

- development of a method to identify the pulse width errors and compensate the wheel speed data for such errors in the event domain
- development of a suitable method to convert the event based wheel speed data to the time domain considering:

- frequency content required for the first tyre resonance frequency estimation
- minimum aliasing of frequencies above the Nyquist frequency in the wheel speed signal

To facilitate this project, raw measurement data of the ABS wheel speed sensors are available including a Simulink interface to assess this data. The data is gathered in a Volkswagen Jetta. This car is equipped with an indirect Tyre Pressure Monitoring System (TPMS) that uses the tyre resonance observed in the wheel speed to give a low inflation pressure warning, meaning that the wheel speed sensors of the car are apparently appropriate for this task. Nevertheless, also an additional high precision wheel speed sensor is mounted on the rear left wheel during several measurements. This sensor can be used for comparison purpose with the available wheel speeds obtained from the low cost ABS wheel speed sensor.

In order to perform the signal processing of the wheel speed sensor, a similar scheme as developed in [7] is used in this research work.

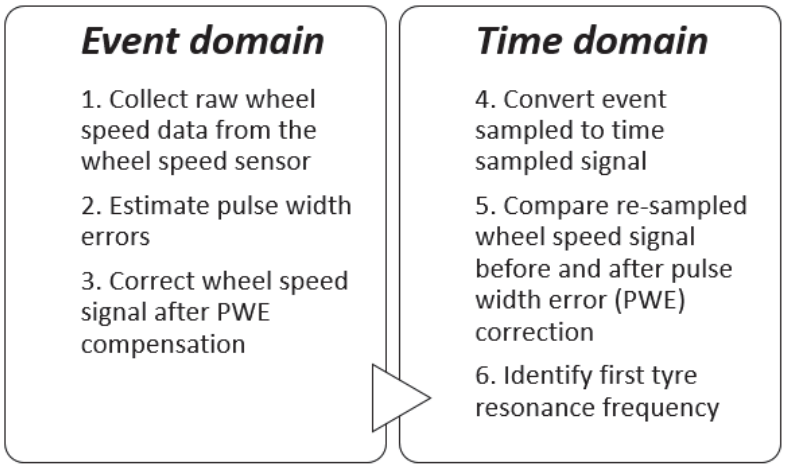

Figure 1.1: Overview of the processing steps.

Figure 1.1 gives a schematic overview of the processing steps in order to process the ABS wheel speed sensor. The wheel speed sensor signal processing is divided into two major phases: event and time domain. The development follows the steps given in Figure 1.1.

1.3 Project approach and outline

In this research, two major phases are identified as shown in Figure 1.1 and the developed method is initially validated using a simulation model at each phase, starting with simple

test cases in the development process. Finally, the developed method for wheel speed sensor processing is applied to measurement data of the vehicle.

An outline of the research work in this report is given for each chapter. **Chapter 2** documents some of the already available research work regarding the wheel speed processing. In **Chapter 3**, the theory behind the working principle of an event based ABS wheel speed sensor together with the problems associated in the sensor are discussed. **Chapter 4** explains the methods used for the conversion of wheel speed signal from the event domain to the time domain. The chapter also discusses the frequency analysis of the re-sampled wheel speed signal. Next in **Chapter 5**, the wheel speed sensor processing method that is developed in this thesis is described. A detailed analysis of the results from the validation of the developed method are also given. Finally in **Chapter 6**, the developed method is applied to vehicle measurement data and the results are analysed. The thesis report ends with conclusions and recommendations for further research in **Chapter 7**.

Chapter 2

Literature Review

Research on tyre-road friction estimation is carried out since the early 1990s. The detection of the friction coefficient for different road surfaces during normal driving conditions is still under development. To tackle the problem of this research project, a brief review of the past research is provided in this chapter. This serves as a baseline for the development of the sensor signal processing method mentioned in this thesis.

Most vehicle control systems like, ABS, ESC, cruise control depends on the wheel speed signal. Besides this, one of the modern systems, which depends on the wheel speed signal is the Indirect Tyre Pressure Monitoring System (TPMS). The first tyre resonance frequency from the wheel speed signal is used as an indirect way of determining the tyre inflation pressure for the TPMS system. This resonance frequency can also be used for the estimation of the tyre-road friction coefficient, which is described in [1], [2] and [3]. Hence, the reliability of these vehicle control systems primarily depends on the quality of the wheel speed signal.

The quality of the wheel speed signal is however reduced due to the periodic disturbances caused by uneven width of the teeth in the sensor toothed wheel, and these are known as Pulse Width Errors (PWE). Hence, identifying the first tyre resonance frequency from the wheel speed signal is a major concern, which has been subject to research since the early 2000s as described in [8], [4] and [9].

The ABS wheel speed sensor does not directly give the wheel speed data. The only information from the sensor are the time instants when an edge of the sensor toothed wheel passes the sensor. Hence, the time period between the last two detected edges are not uniform and this is known as event based sampling. Here, the passage between the detected edges of the toothed wheel are the events. The difference between the time and event based sampling is shown in Figure 2.1.

From Figure 2.1 it can be seen that for event based sampling, the time period between events are not equidistant and is varying as the signals are sampled for constant amplitude.

This is unlike time sampling, where the signals are sampled with constant time period. This example also implies to the ABS sensor, where the time instants are received only when a tooth in the sensor toothed wheel passes the sensor. A more detailed explanation on the ABS sensor and the event based sampling is given in Chapter 3.

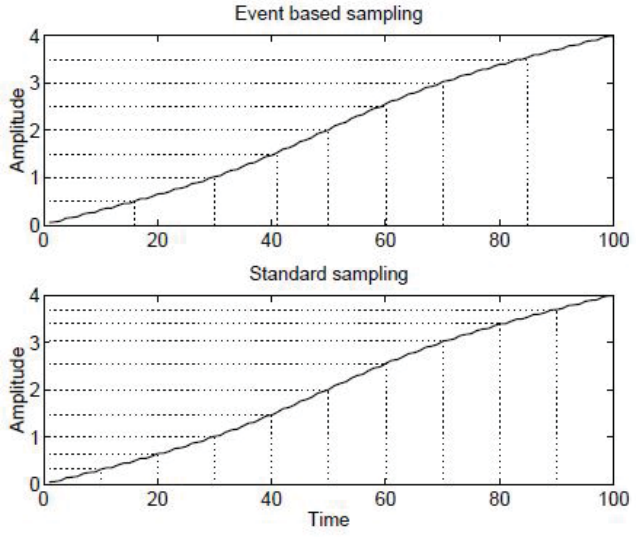

Figure 2.1: Event and Time based sampling [7].

However, as already mentioned, the quality of the wheel speed signal is affected by periodic PWE. The pulse width errors (PWE) occur because of the production tolerances and are repeated in every revolution [10]. The influence of the PWE can be seen if the wheel speed signal with fixed sample period is transformed to the frequency domain and is shown in Figure 2.2.

Figure 2.2 shows the Power Spectral Density (PSD) of the wheel speed signal before and after pulse width error correction, which is as described in [7]. It is concluded from Figure 2.2 (a) that the harmonics seen in the original wheel speed signal are due to the pulse width errors and this is the reason for not able to identify a clear first tyre resonance frequency from the PSD plot.

Hence, in order to extract the resonance frequency information, the pulse width errors need to be eliminated from the wheel speed signal. In [7] and [9], a computationally efficient way to estimate PWE is developed and a method to correct the wheel speed signal is also proposed. The PSD of the wheel speed signal after PWE correction is shown in Figure 2.2(b).

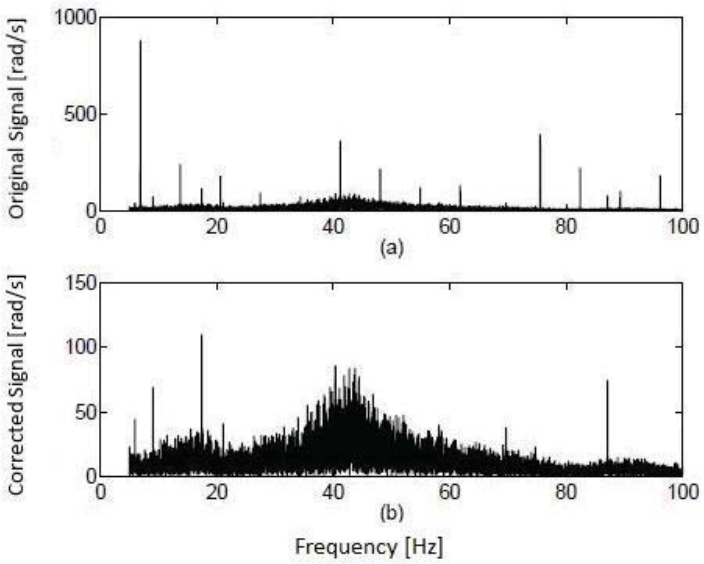

Figure 2.2: (a)Wheel speed signal before PWE correction (b) Wheel speed signal after PWE correction [7].

The PWE is estimated in the event domain using a Recursive Least Squares (RLS) filter. This estimator determines the PWE for every detected edge from the sensor individually. In [7], the developed estimator is studied and tested in a simulation environment for constant wheel speed with a sinusoidal disturbance. It is also shown that after every revolution, the sum of all PWE from the estimator is zero. However, this constraint is not considered in the research work of [7], which when implemented will be useful in order to obtain the PWE at a faster rate. After estimating the pulse width errors for each detected edge, the wheel speed signal is compensated with the obtained PWE in the event domain. Then the signal has to be converted from the event to the time domain. Since the application of the ABS sensor involves event based sampling, the normal sampling theory cannot be used, as the time period in the event sampled signal is not constant. Hence, a time sample period has to be fixed in order to convert the event based wheel speed data with varying time period to a time sampled wheel speed signal. However, an important requirement when choosing the fixed sample period is that the aliasing of frequencies above the Nyquist frequency should be minimized such that the re-sampled wheel speed signal is not affected by a false image due to the aliasing effect.

In [7], different methods of interpolation for converting the event to the time domain are discussed, which are linear and kernel based interpolation. The proposed linear interpolation method is performed by first fixing a low sample period Δt and then interpolating the two consecutive samples of the event based wheel speed data. This further gives the

wheel speed signal with fixed sample period $\Omega_{p\Delta t}$, where p is the number of the sample with fixed sample period Δt. An extension to the linear interpolation is given using kernel based interpolation in [7]. In the case of kernel based interpolation, instead of using two fixed samples in order to calculate $\Omega_{p\Delta t}$, the surrounding neighbourhood of the fixed sample period Δt is considered. However, this method collects samples in the surrounding of Δt by using a design parameter d. This method is given by

$$\Delta t - d < t_k < \Delta t + d \tag{2.1}$$

In (2.1), d is the design parameter which defines the surrounding neighbourhood of interest, k is the sample index in the event domain, i.e. detected edges from the ABS wheel speed sensor. t_k is the time instants for each sample. The samples in the surrounding neighbourhood are computed using the Epanechnikov kernel function and it has to be carefully considered. The kernel approach can be seen as a low pass filter, where design parameter d can be referred as a cut-off frequency in the filter. However, the complexity in the method will increase, when the number of samples increases in the neighbourhood of Δt. This happens when the wheel speed is varying.

Summary

The functionality of many vehicle control systems depends on the wheel speed signals. The steps in the event and the time domain phases for processing the wheel speed sensor signal are discussed in this chapter based on the work of [7].

For the estimation of the pulse width errors in the event domain, an adaptive algorithm is implemented by [7]. The pulse width errors for each detected edge is estimated using a recursive least squares filter (RLS). Extension of the RLS filter by considering the constraints in the estimator is proposed in Chapter 3. Moreover, the RLS filter to estimate the PWE is limited to constant wheel speed condition in [7]. Hence, in this thesis, the RLS filter is also evaluated for varying wheel speed condition in order to estimate PWE, which is explained in Chapter 5.

Converting the wheel speed signal from the event domain to the time domain is the major concern as there is no specific method to accomplish the task. Based on the work of [7], the linear interpolation is reconsidered in this thesis, as the kernel based interpolation is complex while implementing in real time. An extension to the linear interpolation by using a cubic polynomial interpolation method is implemented in Chapter 4. In addition to the cubic polynomial interpolation, an integrated sampling approach is also proposed for converting the signal from the event domain to the time domain.

At each phase, the wheel speed signal processing method is validated in order to identify the problems and correct it. The developed processing method is validated for both simulation and vehicle measurement data in this thesis.

Chapter 3

Event Based Wheel Speed Estimation

This chapter explains the theoretical aspects of the signal processing for an event based ABS wheel speed sensor. The chapter also presents a method to eliminate the pulse width errors from the wheel speed signal in the event domain. A case for testing the method developed to correct for pulse width errors is given in the last section.

3.1 The ABS wheel speed sensor

The wheel speed sensor measures the wheel speed, [1] using an inductive sensor, detecting each tooth edge of a rotating toothed wheel. The toothed wheel is connected to the wheel or the drive shaft. A pulse is generated when a tooth in the toothed wheel passes the sensor. The sensor signal is converted to a square wave with constant amplitude and the edges in the signal represent the edges of the toothed wheel. The working principle of the sensor is also shown in Figure 3.1.

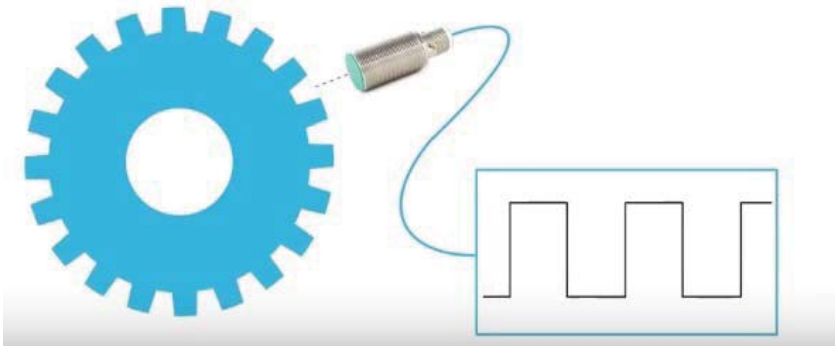

Figure 3.1: Working principle of an inductive wheel speed sensor.

[1] Angular velocity of the wheel is referred as wheel speed in this report.

The continuous signal from the sensor will be discretized before further processing. For this reason, a microprocessor is connected with the sensor. This microprocessor consists of a clock with fixed clock sample period Δt_{clock}, a timer and a counter. A counter is a device in a microprocessor, which records the number of occurrences of an event. A timer in the microprocessor records the time instances for every event, which further depends on the fixed clock sample period Δt_{clock}.

In this case, at every clock period, the value of the timer is increased. When the toothed edge passes the sensor as shown in Figure 3.1, the corresponding timer value is stored into a measurement vector. The more frequently the clock period occurs, the more accurate is the value of time instants. Hence, an event in the wheel speed sensor occurs when a tooth passes the sensor. As soon as an event is passed, the counter records the corresponding event number. The toothed wheel of an ABS wheel speed sensor is given in Figure 3.2. The calculation of the instantaneous wheel speed is represented by

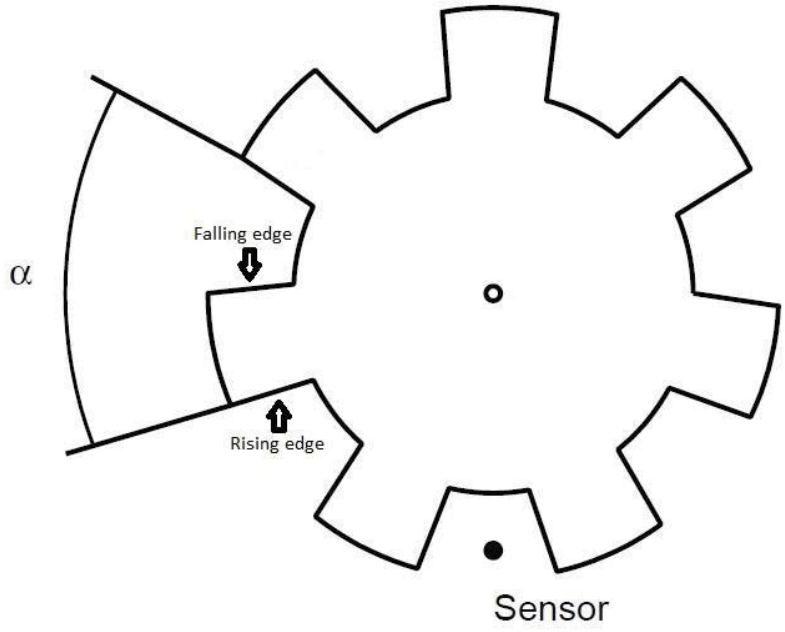

Figure 3.2: Toothed wheel of an ABS wheel speed sensor [7].

$$\Omega_{i,k} = \frac{\alpha}{(t_k - t_{k-1})} \tag{3.1}$$

Where, the angle between last two detected edges is α. In (3.1), k represents the detected edge and $k-1$ represents the previous edge. $\Omega_{i,k}$ represents the instantaneous wheel speed at every detected edge. Subscript i represents instantaneous condition, i.e wheel speed is measured at every time instants. t_k and t_{k-1} represents the time instants of the last two

detected edges. Δt_k is the difference between the two time instants t_k and t_{k-1} in the instantaneous case. The computation of the angle is given as

$$\alpha = \frac{2\pi}{N_{edge}L} \tag{3.2}$$

Here, L represents the total number of teeth in the toothed wheel and N_{edge} represents the number of edges detected by the sensor for each tooth. N_{edge} can either be 1 or 2 depending on the type of ABS sensor used. If N_{edge} is 2, it means that for each tooth the rising and falling edges are detected and if the value is 1, it means that either the rising edge or the falling edge is detected. Further, $N = N_{edge}L$, and N is the total number of detected edges by the sensor in the toothed wheel for one revolution. From Figure 3.2, it is clear that an event occurs when the last two detected edges passes the sensor, i.e. when the angle α is crossed in the toothed wheel. Hence, the ABS wheel speed sensor follows an event based sampling approach.

3.2 Sampling Methods: Time and Event based

Time based sampling: In this sampling technique, a continuous signal $x(t)$ is sampled at fixed sample period Δt and the resultant sampled information is stored as amplitudes.

$$x_p = x(p\Delta t) \tag{3.3}$$

Here, x_p is the sampled signal i.e amplitude of the continuous signal at multiples of the fixed sample period Δt. p is the number of the sample with fixed sample period Δt and $p = 1, 2, 3....$

Event based sampling: An event occurs when the amplitude of the signal reaches a pre-determined level. Hence, the signal is sampled only when an event occurs and this is referred to as an event based sampling [7], [11]. The sampled information is stored as time instants t_k unlike the time based sampling method, where the sampled information is stored as an amplitude. Event based sampling is non-uniform, where the time period varies for each event. Thus, re-sampling from event to time domain cannot be done by conventional sampling theory and needs some approximation methods. Event based sampling has many advantages in the the application of motion control systems, where the controls are not executed unless it is actually required.

$$x(t_k) = x_k \tag{3.4}$$

(3.4) represents event based sampling for the signal. x_k represents the pre-determined amplitudes at time instants t_k. k is the sample index or event index where, $k = 1, 2, 3...N$.

3.3 Non-ideal toothed wheel

In an ideal condition, the wheel speed is calculated according to (3.1) however, in practical cases, this is not true. The toothed wheel always has small pulse width errors (PWE) due to the production tolerances or distortion i.e. width of the teeth may not be uniform [8]. This is represented as the non-ideal toothed wheel and is shown in Figure 3.5. As already mentioned, the only output from the sensor are the time instants t_k. From Figure 3.5, the time instants t_k and t_{k-1} are received for a non-ideal tooth. Thus, the angle α is not the same and is influenced with the unknown PWE. Pulse width errors (PWE) δ_k may be seen at each detected edge, and since the wheel is rotating, these errors are periodic with wheel rotation. In Figure 3.5, it can be seen that the sensor gives time instants t_k for only one edge per tooth. Hence, the PWE is also seen at only edge in every tooth [8]. The influence of PWE when computing the wheel speed can be represented by

$$\Omega_{c,k} = \frac{\alpha \pm \delta_k}{\Delta t_k} \tag{3.5}$$

From (3.5), $\Omega_{c,k}$ represents the computed wheel speed from the wheel speed sensor and subscript c represents computed. However, when computing the wheel speed as given by (3.5), the PWE term δ_k may be unknown. Hence, the primary objective is to identify the unknown PWE δ_k.

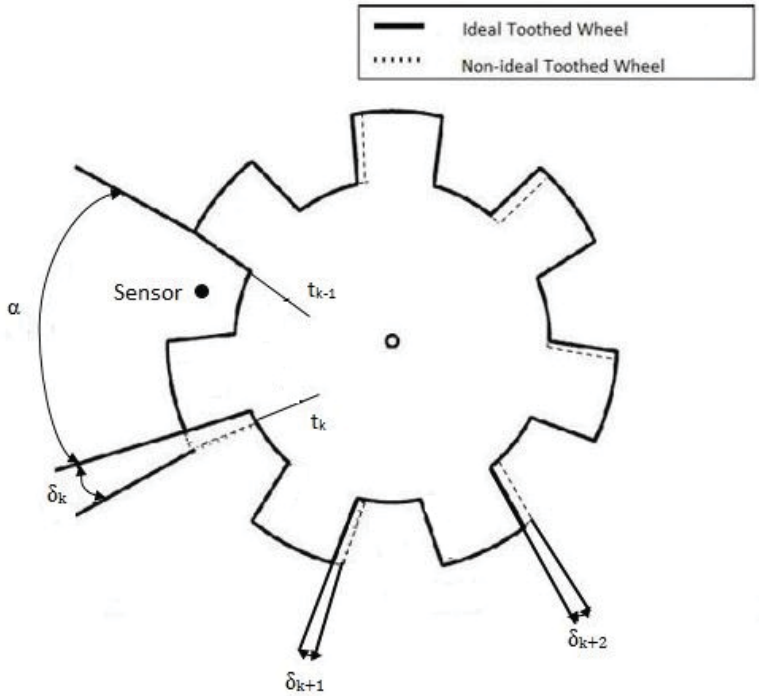

Figure 3.3: Non-ideal toothed wheel with pulse width errors [7].

An important assumption is that the wheel speed variations due to pulse width errors will dominate the disturbance in the wheel speed signal, and hence, other disturbances due to non uniformity of the tyres, suspension, etc are thus negligible [9]. When the wheel speed is constant, the pulse width errors are seen as clear harmonics in the frequency domain [10]. Since these harmonics occur only at certain specific frequencies in the signal, these can be computed from the fundamental frequency f_{fund} represented by

$$f_{fund} = \frac{\Omega_{c,k}}{2\pi} \tag{3.6}$$

From (3.6), PWE for every detected edge are observed at each multiple of the fundamental frequency f_{fund} and, this can be seen as higher harmonics in the frequency domain. With varying wheel speed, the pulse width errors get distributed differently in the frequency domain and it is hard to observe the required resonance frequency from the wheel speed data [7]. Hence, estimation and correction of pulse width errors are very important in the processing of wheel speed.

3.4 Estimation of pulse width errors in the event domain

The objective of the estimation technique is to determine the pulse width errors δ_k for every detected edge and to correct the computed wheel speed signal $\Omega_{c,k}$. The estimation technique, as described in [7], treats the pulse width errors in each detected edge individually. An adaptive recursive least square algorithm is used, which estimates the pulse width error for all detected edges of the teeth after every revolution. The overall idea of the algorithm for estimating PWE is to derive a vector, which contains one element for every detected edge. Then this vector can be used for correcting the wheel speed signal in the event domain.

The working principle of the RLS filter: The RLS estimator iteratively updates the unknown parameter to be estimated at each step with the data from the past. The interplay between the system and the RLS estimator is presented in Figure 3.4. In Figure 3.4, θ_k represents the parameter to be estimated recursively and, $\hat{\theta}_k$ represents the estim-

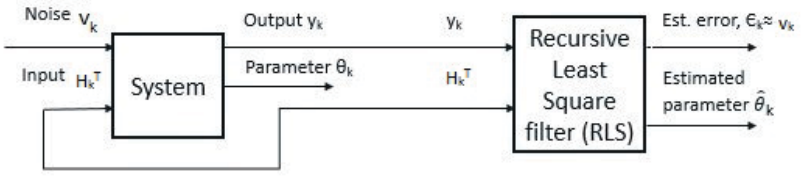

Figure 3.4: Interplay between system and RLS estimator.

ated parameter. v_k is the system noise, which is unknown, and H_k^T represents the input regression vector. The linear regression model for the RLS estimator is written below:

$$y_k = H_k^T \hat{\theta}_k + \varepsilon_k \tag{3.7}$$

In (3.7) and Figure 3.4, y_k represents the measurement output and ε_k is the estimation error. The model output from the RLS estimator is compared with the measurement output, which in turn gives the estimation error ε_k. This error is used to estimate the parameter adaptively. The estimation error ε_k is defined as the difference between measurement output at the present data and the model output from estimated parameters of the previous data [12]. H_k^T is the input regression vector. This error is calculated as shown below

$$\varepsilon_k = y_k - H_k^T \hat{\theta}_{k-1} \tag{3.8}$$

Furthermore, the sum of the squares of the measurement error ε_k is the optimality criterion for the cost function J_k to be minimized and is represented as shown below:

$$J_k = \sum_{j=1}^{k} \lambda^{k-j} (\varepsilon_k)^2 \tag{3.9}$$

In (3.8), λ represents the forgetting factor which is a positive constant close to, but less than, 1. The forgetting factor is to ensure that the past data are forgotten and the output estimate is obtained quickly. The inverse of $1 - \lambda$ is considered to be the memory of the system [13]. The procedure of the RLS estimator is as follows:

- Initializing the estimator: The unknown parameter to estimate θ_k, and the covariance matrix of the estimate,P_k are first initialized. The initial values are prescribed in order to update the parameter to estimate from the past data. The initial estimate $\hat{\theta}_0$ is an approximate value, which is usually taken by guessing the value of the output estimate. If the value of the output estimate is not known, then $\hat{\theta}_0$ can be taken as 0. The initial covariance P_0 on the other hand depends on a regulation parameter, γ^{-1}. The regulation parameter is the tuning parameter for a faster convergence of the output estimate.

  $$P_0 = \gamma^{-1} I \tag{3.10}$$

  The regulation parameter, γ^{-1} depends on the accuracy of the initial estimate with that of the output estimate. If the confidence on the selection of the initial estimate $\hat{\theta}_0$ value is high, then the values in the initial covariance matrix P_0 is set to a smaller value, i.e. the regulation parameter can be a small value. Similarly, if the confidence in choosing $\hat{\theta}_0$ is low then, P_0 is taken a higher value [14]. If P_0 is very close to zero, then the estimator assumes that there is no error and outputs the same value as the initial estimate.

- The measurement output y_k and the input regression H_k^T are computed, and sent as inputs to the estimator.

- Then the estimation error ε_k is computed.
- After that, the gain matrix K_k and the covariance matrix, P_k are updated as follows:

$$K_k = \frac{P_{k-1}H_k}{\lambda + H_k^T P_{k-1} H_k} \tag{3.11}$$

$$P_k = \frac{1}{\lambda}(P_{k-1} - K_k H_k^T P_{k-1}) \tag{3.12}$$

  The covariance matrix P_k determines the direction for the convergence of the output estimate $\hat{\theta_k}$. The inverse of the covariance matrix from the previous data P_{k-1} in (3.12) makes the covariance matrix P_k of the current data, non singular, and hence P_k keeps on increasing or decreasing monotonically.

- Next, the parameter to be estimated $\hat{\theta_k}$ is updated from the previous estimate $\hat{\theta}_{k-1}$ with a correction term. The correction term is the estimation error ε_k multiplied with the gain matrix K_k.

$$\hat{\theta_k} = \hat{\theta}_{k-1} + K_k \varepsilon_k \tag{3.13}$$

3.4.1 Revolution based RLS estimator

The revolution based RLS estimation algorithm works similar as a normal RLS estimator. It works on the principle that the estimator gives the pulse width error estimates for every complete revolution of the toothed wheel.

On comparing the RLS estimator with the revolution based RLS estimator, the estimated parameter $\hat{\theta_k}$ is the pulse width error δ_k. (3.7) representing the measurement output of the RLS estimator, is compared and further represented for the revolution based RLS estimator as follows:

$$\begin{bmatrix} y_1 \\ y_2 \\ y_3 \\ . \\ . \\ . \\ . \\ . \\ . \\ y_N \end{bmatrix} = \begin{bmatrix} 1 & 0 & 0 & . & . & . & . & . & 0 \\ 0 & 1 & 0 & . & . & . & . & . & 0 \\ 0 & 0 & 1 & . & . & . & . & . & 0 \\ . & & & 1 & & & & & . \\ . & & & & 1 & & & & . \\ . & & & & & 1 & & & . \\ . & & & & & & 1 & & . \\ . & & & & & & & 1 & 0 \\ 0 & & & & & & & & 1 \end{bmatrix} \begin{bmatrix} \delta_1 \\ \delta_2 \\ \delta_3 \\ . \\ . \\ . \\ . \\ . \\ \delta_N \end{bmatrix} + \begin{bmatrix} \varepsilon_1 \\ \varepsilon_2 \\ \varepsilon_3 \\ . \\ . \\ . \\ . \\ . \\ \varepsilon_N \end{bmatrix} \tag{3.14}$$

In Equation (3.14), δ_k represents the value of pulse width error at each detected edge. (3.14) can be further represented for one revolution as shown by

$$y_r = H_r^T \hat{\theta}_r + \varepsilon_r \tag{3.15}$$

From Equation (3.15) y_r represents the measurement output for all the detected edges in one revolution of the toothed wheel, which is a [N x 1] matrix. $\hat{\theta_r}$ represents the estimated parameter for all detected edges in one revolution and it is a [N x 1]. The parameter estimate $\hat{\theta_r}$ gives the PWE values for all detected edges δ_k and r represents "revolution" in the equation. H_r^T represents the input regression matrix for one revolution, which is a [N x N] matrix. Similarly ε_r is the estimation error for all detected edges in one revolution and represents a [N x 1] matrix. The same procedure mentioned for computing the estimate using the RLS filter is used for the revolution based RLS estimator. Once in every revolution, the PWE, the covariance matrix and the gain matrix for all detected edges is updated by the revolution based RLS.

The measurement output, y_k for each detected edge in the revolution based RLS method is computed and given by

$$y_k = \alpha - \hat{\Omega_k^0}\Delta t_k \tag{3.16}$$

From (3.16), $\hat{\Omega_k^0}$ represents the reference wheel speed, which is the estimated current wheel speed for every detected edge. According to (3.16), the measurement output y_k results in the values of the pulse width errors δ_k for each detected edge as it measures the difference between the ideal angle and the computed angle. The reference wheel speed is computed as shown by

$$\hat{\Omega_k^0} = \frac{2\pi}{(t_k - t_{k-N})} \tag{3.17}$$

In (3.17), $(t_k - t_{k-N})$ represents the time period for one complete revolution. Hence, it can be seen that the reference wheel speed for every event depends on the previous revolution data [9]. For the first revolution, it is assumed to start from rest, since in reality, the vehicle is always started from rest. For a standard ABS wheel speed sensor, the variations due to PWE have a much higher frequency content than the wheel speed variations due to the suspension and road unevenness [10]. Hence, it is assumed that during one revolution, reference wheel speed may be considered as a constant value. It is also considered that the variations due to suspension and road unevenness are stochastic in nature, while PWE are periodic with wheel rotation. However, there is always a bias in the reference wheel speed computation given by (3.17), since it assumes that the wheel speed is almost constant for one revolution. These bias in the estimation of the reference wheel speed may be negligible when the wheel speed is constant but have some impact when the wheel speed is varying. The bias in the reference wheel speed computation may also be observed in the estimation error values when the wheel speed is varying or drops drastically when a wheel locks up due to braking.

This estimation algorithm estimates pulse width errors only after one full revolution of the toothed wheel. Hence in the estimation of PWE according to (3.14), there is a constraint that has to be dealt with. From (3.14), the sum of all pulse width errors in one revolution are constrained to be zero.

$$\sum_{k=1}^{N} \delta_k = 0 \tag{3.18}$$

However, since a prior knowledge on the sum of all PWE in one revolution is already known, it is advisable to apply the constraint equation after every revolution of the toothed wheel. This constraints can be implemented with the proposed revolution based RLS estimator using (3.19) as shown by

$$A\hat{\theta}_r = B \tag{3.19}$$

From (3.19), A represents the known constraint matrix and B is also a known vector, which is the so-called response vector. Since the sum of all δ_k is zero, A takes the value [1 1....1], which is a [1 x N] matrix. The resultant response vector B takes the value 0, which is a known result. (3.19) can be combined with (3.14) in order to evaluate the revolution based RLS model with constraints and is shown as

$$\begin{bmatrix} y_1 \\ y_2 \\ y_3 \\ . \\ . \\ . \\ . \\ . \\ y_N \\ 0 \end{bmatrix} = \begin{bmatrix} 1 & 0 & 0 & . & . & . & . & . & 0 \\ 0 & 1 & 0 & . & . & . & . & . & 0 \\ 0 & 0 & 1 & . & . & . & . & . & 0 \\ . & & & 1 & & & & & . \\ . & & & & 1 & & & & . \\ . & & & & & 1 & & & . \\ . & & & & & & 1 & & . \\ 0 & & & & & & & 1 & 0 \\ 0 & & & & & & & & 1 \\ 1 & 1 & 1 & 1 & 1 & 1 & 1 & 1 & 1 \end{bmatrix} \begin{bmatrix} \delta_1 \\ \delta_2 \\ \delta_3 \\ . \\ . \\ . \\ . \\ . \\ \delta_N \end{bmatrix} + \begin{bmatrix} \varepsilon_1 \\ \varepsilon_2 \\ \varepsilon_3 \\ . \\ . \\ . \\ . \\ . \\ \varepsilon_N \\ 0 \end{bmatrix} \tag{3.20}$$

Comparing (3.20) with (3.15), H_r^T is a [N+1 x N] matrix, ε_r is a [N+1 x 1] and y_r is also a [N+1 x 1] matrix. $\hat{\theta}_r$ represents the PWE for all detected edges in one revolution and it is a [N x 1].

Two simple examples to show the performance of the RLS estimator with and without constraints are given below. The RLS estimator with constraints is computed based on (3.20) and the RLS estimator without constraints is computed based on (3.14).

Example 3.1

In this example, a toothed wheel of the ABS sensor is assumed with total number of teeth L=43 and the number of detected edges at each tooth, N_{edge} =1. Hence, there are 43 detected edges in this case. A constant wheel speed of 50 rad/s is considered and there is no disturbance in the wheel speed. The reference wheel speed for every detected edge is assumed to be the same as the constant wheel speed. Further, a set of random pulse width errors δ_k are introduced for each detected edge, and these are added to the angle α when computing the time period Δt_k. Now the time period for each edge is influenced

by the PWE. The computed time period Δt_k, and the reference wheel speed is taken as input to the revolution based RLS estimator. The initial parameter estimate $\hat{\theta}_0$ and initial covariance P_0 for the RLS estimator are assumed to be 10^{-3} and I_{43}. The forgetting factor for each detected edge is taken to be 0.9995. 1000 revolutions are considered for this Example. The resultant PWE estimate δ_k is shown in Figure 3.5.

In this Example, the revolution based RLS estimator is modelled with and without constraint, i.e as represented in (3.14) and (3.20), and are separately evaluated. From Figure 3.5, it can be observed that the estimated values of the PWE for RLS with and without constraint, converges with the introduced values of the PWE. The pink dot is the initial estimate, $\hat{\theta}_0$ for the estimator. An accurate convergence is possible as there are no external disturbances and also the reference wheel speed is assumed to be constant. The major advantage of using the constraint equation in the model is to emphasize that if a prior knowledge is known in the estimation, the convergence of the PWE estimate is quicker. The performance of the estimator is further illustrated when checking the covariance matrix, which is shown in Figure 3.6.

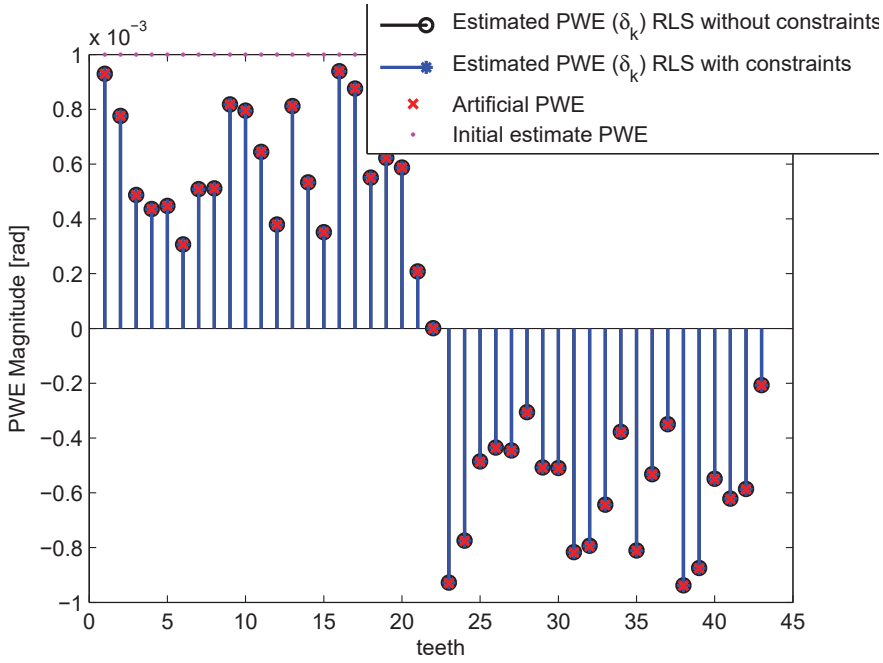

Figure 3.5: Estimation of pulse width errors for all detected edges with and without constraint.

In Figure 3.6(a) and (b), the covariance matrix for revolution based RLS estimator with and without constraint is shown. It can be seen for this example that the covariance matrix converges monotonically to a lower value. This further confirms that the revolution based RLS model with and without constraint can work for the simple case of constant wheel

speed.

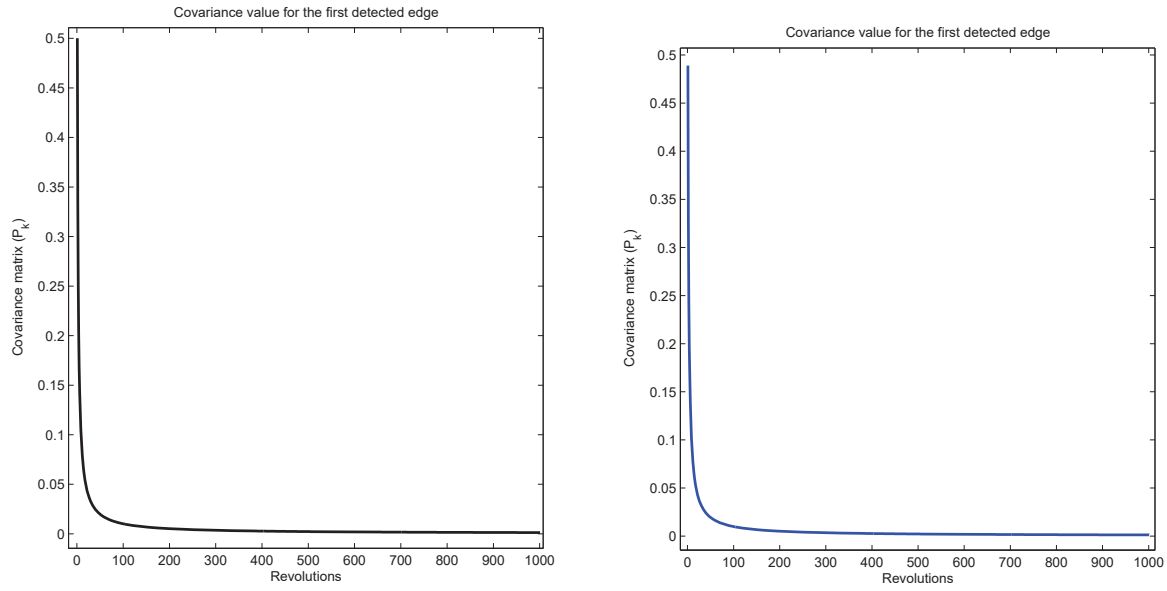

(a) (b)

Figure 3.6: (a)Covariance matrix value for the first detected edge without constraint (b)Covariance matrix value for the first detected edge with constraint.

Some ABS sensors gives time instants for two edges in one tooth i.e for both rising and falling edges. Hence, there will 86 edges in one revolution. This case is evaluated for RLS estimator with and without constraints in Example 3.2.

Example 3.2: Assuming a toothed wheel of the ABS sensor with a total number of teeth L=43 at a constant wheel speed of 50 rad/s and the number of detected edges at each tooth, N_{edge} =2. Similar to Example 1, random PWE for 86 edges are introduced with angle α when computing the time period Δt_k. The RLS estimator is again made to run for 1000 revolutions. The initial parameter estimate $\hat{\theta_0}$ and initial covariance P_0 for the RLS estimator are assumed to be 10^{-3} and I_{43}. The forgetting factor for each detected edge is taken to be 0.9995. The resultant PWE estimate from the revolution based RLS estimator is shown in Figure 3.7.

Figure 3.7 shows the performance of the revolution based RLS estimator with and without constraint for estimating PWE at 86 detected edges. From Figure 3.7, it can be seen that the PWE estimate from the revolution based RLS estimator without constraint agrees with the introduced PWE values.

However, the PWE estimate from RLS model with constraint does not agree with the

introduced PWE values. This is further evaluated by analysing the covariance matrix for the RLS estimator with and without constraints. This is shown in Figure 3.8. The covariance value is shown only for the first detected edge.

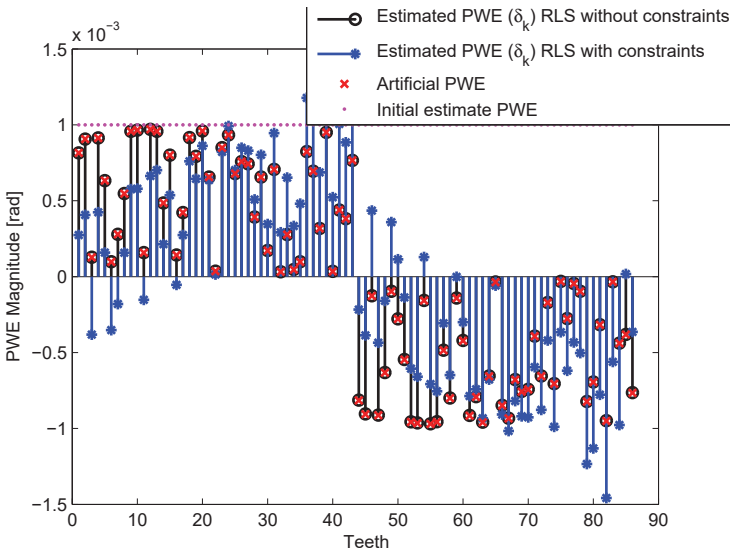

Figure 3.7: Estimation of pulse width errors for all detected edges with and without constraints.

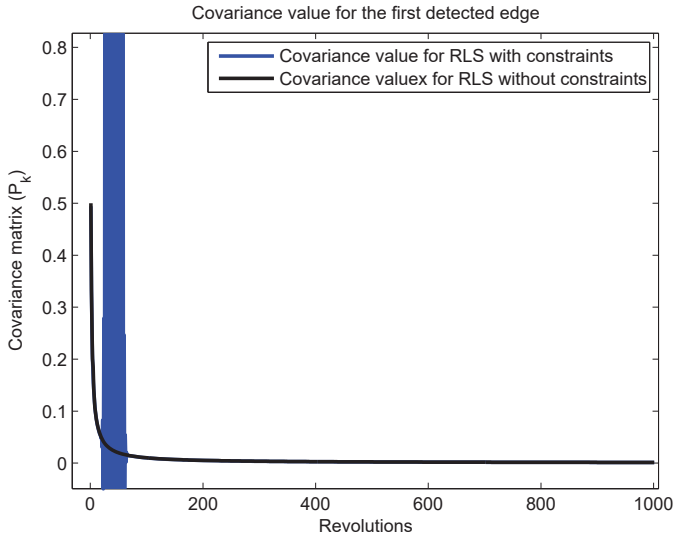

Figure 3.8: Covariance matrix value for the first detected edge with and without constraints.

In Figure 3.8, it can be seen that the covariance value for the first detected edge, decreases monotonically for the RLS model without constraint (shown in black). Furthermore, the covariance matrix is converged to its lowest value after around 300 revolutions. However, when the estimator is modelled with constraint as given by (3.20), the covariance value for the first detected edge rapidly increases to a high value after 20 revolutions.

After around 65 revolutions, the covariance value for the model with constraint, converges with covariance value for the model without constraint. Similar kind of rapid increase in values is also seen in the estimation error for all detected edges. This occurs when the magnitude of the detected edges increases. Here, a forgetting factor of 0.9995 for every detected edge is taken. Reducing the forgetting factor less than 0.9995 worsens the estimated value of PWE. Increasing the forgetting factor to 1 also gives the same overshoot in the covariance value between 20 and 65 revolutions. A clear reason for this overshoot could still not be identified. In order to implement a constraint with RLS estimator for this application, (3.20) might not be an optimal approach.

Conclusion from the revolution based RLS estimator: Revolution based RLS model is modelled with and without constraint. However, the constraint equation could not be updated recursively when modelled as given by (3.20). Hence, the RLS estimator with constraint is not considered for further validation. Furthermore for the RLS estimator without the constraint, various cases are analysed and presented in the Section 3.4.2 and also in chapter 5.

3.4.2 Artificial test case 1: Constant wheel speed

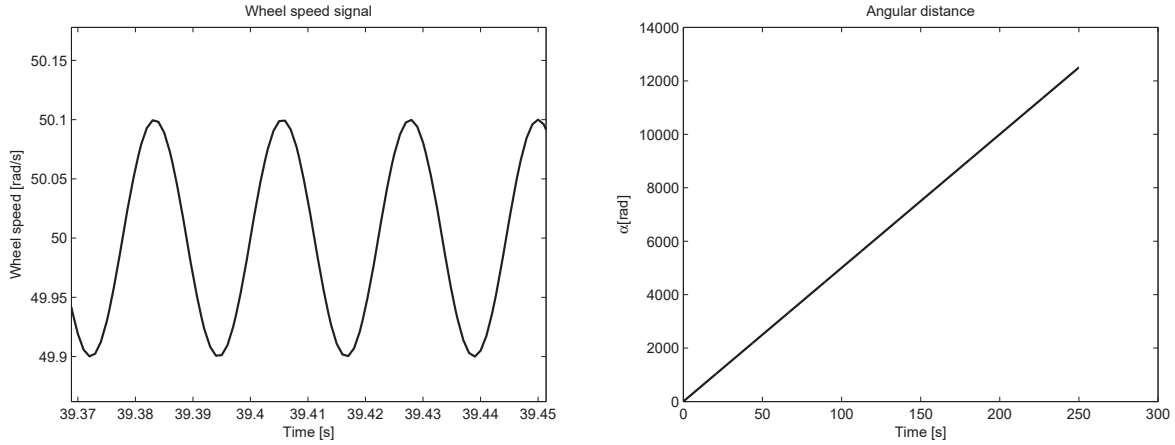

(a) (b)

Figure 3.9: (a)Wheel speed signal (b)Angular distance signal.

Assume a toothed wheel in the ABS wheel speed sensor with total number of teeth i.e. L=43 rotating at a constant wheel speed of 50 rad/s. A signal component $s(t) = 0.1sin(2\pi ft)$ with frequency 45 Hz, added to the constant wheel speed signal. t represents the time for the test case and the total time equals 250 s. The sample time in the simulation is set to 0.001 s. The signal component at 45 Hz is aimed to mimic the first tyre resonance frequency. The number of detected edges for every tooth N_{edge} is assumed to be 1. Random pulse width errors (PWE) are artificially introduced, in order to visualize the effect of such errors on the wheel speed signal from the sensor, and also to check the robustness of the revolution based RLS estimator. The sum of all the PWE is assumed to be zero. Hence, the introduced PWE δ_k is taken to be both positive and negative values. The largest value of the pulse width error is taken to be 1% of the α value, which corresponds to the actual value of PWE seen on real world cases [7].

Figure 3.9 (a) represents the input wheel speed signal and it is shown only for limited time in order to clearly see the sinusoidal disturbance. Figure 3.9 (b) represents the angular distance α of the input wheel speed signal. Now the wheel speed and angular distance signal are in the time domain without any pulse width errors. However, to obtain time instants with varying time period, the angular distance profile is event based sampled at every $\alpha - \delta_k$ in order to convert the signal from the time to the event domain. The resultant values from the event sampled signal are the time instants for every $\alpha - \delta_k$. The general equation for introducing the PWE and calculating the events from the time based signal is given by

$$\alpha_k = m2\pi + k\alpha - \sum_{j=1}^{k} \delta_j \tag{3.21}$$

Where, m is the revolution counter, which starts at zero. When the total number of detected edges N is reached, m value is incremented. For example, in the first revolution with 43 detected edges, the event based sampling with influence of PWE in artificial cases is performed as:

$$\begin{pmatrix} \alpha_1 \\ \alpha_2 \\ . \\ . \\ . \\ \alpha_{43} \end{pmatrix} = \begin{pmatrix} \alpha - \delta_1 \\ 2\alpha - \delta_1 - \delta_2. \\ . \\ . \\ . \\ 43\alpha - \delta_1 - .....\delta_{43} \end{pmatrix} \tag{3.22}$$

After every revolution, 2π is added to the detected edges from the previous revolutions. When converting the data to the event domain, the time period from the time instants for every event is computed. This is further used as input for the revolution based RLS estimator in order to estimate the introduced PWE values.

Design parameters: The pulse width errors are not supposed to change over time. If

more past data is forgotten, the estimator becomes very sensitive to numerical errors, causing the output parameter estimate to become more oscillatory. This is solved by selecting a higher forgetting factor of 0.9995 in the estimator for every detected edge. The initial estimate for the PWE in all detected edges is taken to be a value of 10^{-3} rad and the initial covariance P_0 is assumed to be an identity matrix I_{43}. As already explained, when the confidence of the initial estimate is high, the initial covariance matrix can be set to a low value. In the application of the ABS wheel speed sensor, it is known that the PWE is in the magnitude of 10^{-4} rad, so the initial estimate $\hat{\theta_0}$ is taken to be 10^{-3} rad. Since an exact value of the PWE estimate is not known, the confidence on the initial estimate $\hat{\theta_0}$ is very low. Furthermore, the variance of the estimate is not known and, hence, the initial covariance matrix p_0 is chosen to be an identity matrix, i.e. regulation parameter γ^{-1} is 1.

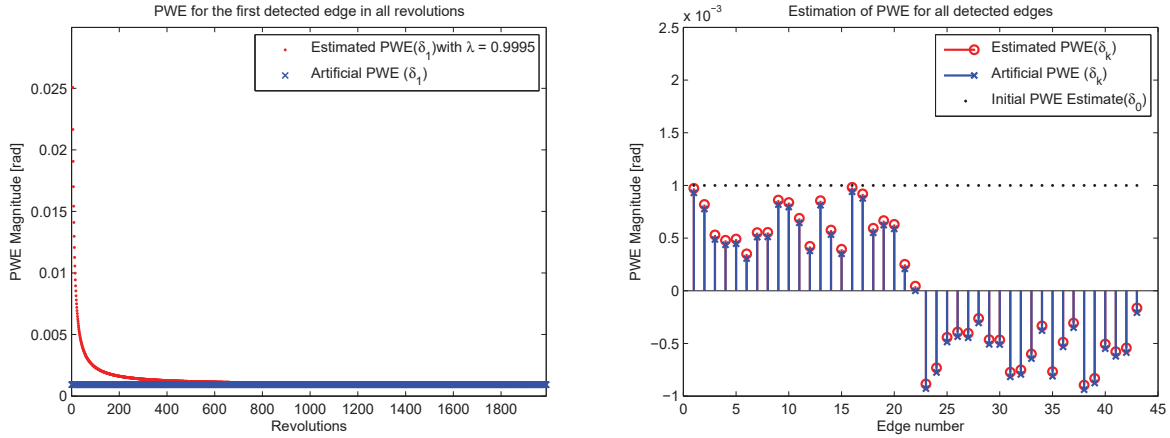

(a) (b)

Figure 3.10: (a)Convergence of estimated and the artificial pulse width errors for the first detected edge in all revolutions (b) Estimation of pulse width errors for all detected edges.

Figure 3.10(a) shows the estimation of PWE for the first detected edge δ_1 of the toothed wheel. In Figure 3.10 (a), it can be observed that the estimated values of the δ_1 converges closer to the artificial values with an accuracy of over 95% at the end of the simulation, which is at the 1990th revolution. The accuracy is determined by computing the difference between the prescribed and the estimated values of PWE. A faster convergence of the PWE cannot be obtained as the estimation of the PWE happens slowly, since a higher forgetting factor is used. Also an initial error in the reference wheel speed computation assuming the fact of one revolution delay affects the accuracy of the estimate. Hence, only 95% accuracy on the PWE estimate can ideally be used for correcting the wheel speed signal. Moreover the values of the PWE for all detected edges is logged at the last revolution, i.e. at the 1990th revolution for correcting the wheel speed signal. The estimate at the last revolution is shown in Figure 3.10(b). The accuracy of the estimated values is further analysed after correcting the wheel speed signals with these estimates in the event domain, which is shown in Figure 3.12(a) and (b).

Convergence criteria: The revolution based RLS estimator updates the pulse width errors at each revolution in order to minimize the sum of the squares of the estimation errors. As previously explained, the cost function J_k is minimized based on the estimation error ε_k at each update [14]. Hence, the performance of the revolution based RLS estimator is checked based on the minimization of the estimation errors and, also by the monotonicity of the covariance value of each detected edge. From Figure 3.11 (a), 95% accuracy from the estimator can be concluded as the squared estimation error $(\varepsilon_k)^2$ drops to a low value close to zero. Similarly, for the covariance matrix at each detected edge, it can be seen that it is divided by the forgetting factor λ at each update, which is shown in (3.12). Hence, the covariance value converges monotonically after certain revolutions, which is another criterion for illustrating the convergence accuracy of the revolution based RLS estimator. The resultant covariance value for the first detected edge in the entire revolutions is shown in Figure 3.11 (b).

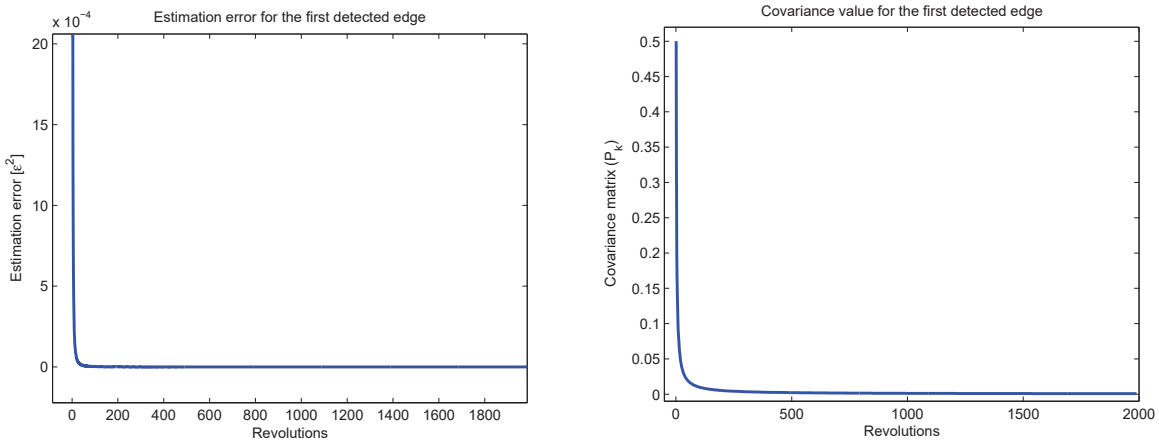

(a) (b)

Figure 3.11: (a)Estimation error for the first detected edge in all revolutions (b) covariance value for the first detected edge in all revolutions.

As it is observed that the pulse width error estimation works with a reasonable accuracy, the computed wheel speed signal as given in (3.5) can be compensated with the estimated PWE, in order to obtain a PWE free signal in the event domain. However, as already explained, the measurement output computes the difference between the ideal and the real angle, which further results in pulse width errors. The estimated PWE consists of both positive and negative values as in one revolution of the toothed wheel, sum of all PWE is zero. Hence, a general format for compensating the wheel speed signal with the estimated PWE is given by

$$\Omega_k = \frac{\alpha - \delta_k}{\Delta t_k} \tag{3.23}$$

In (3.23), Ω_k represents the corrected wheel speed at every detected edge.

Figure 3.12 (a) and (b) show the wheel speed signal before and after PWE corrections for the entire revolutions of the toothed wheel. The wheel speed signal with the influence of PWE can be observed in Figure 3.12 (a)(shown in blue). It can also be seen that the influence of the PWE is eliminated in the corrected wheel speed signal (shown in red) and a closer look of the corrected wheel speed signal Ω_k at every detected edge for one full revolution is shown in Figure 3.12 (b). The corrected wheel speed signal for every detected edge in the event domain Ω_k with respect to time instants is shown in Figure 3.13. The processing method is validated in the event domain by comparing the corrected wheel speed signal with that of the input wheel speed signal from Figure 3.9(a). The comparison is represented in Figure 3.13.

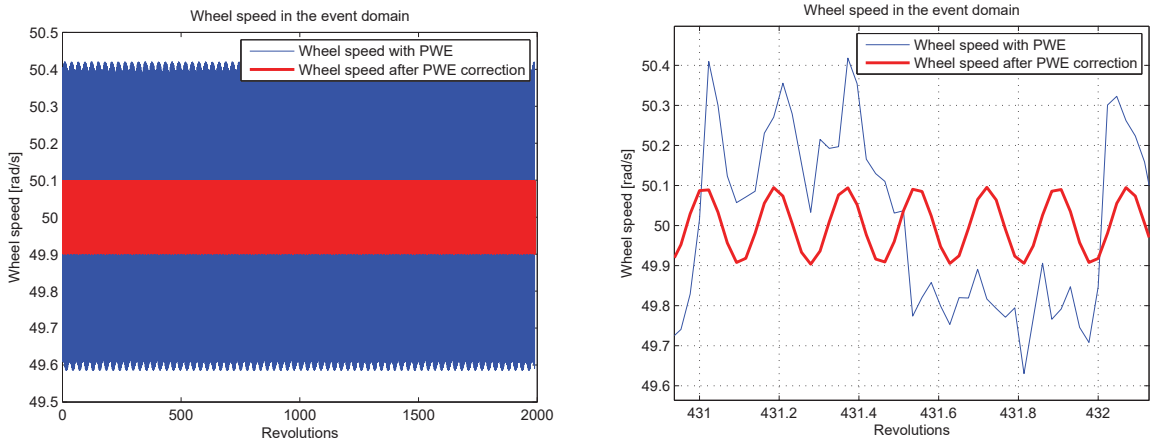

(a) (b)

Figure 3.12: (a)Wheel speed in the event domain before and after PWE correction for the entire revolutions (b) Zoomed-in image.

In Figure 3.13, it can be observed that the time period Δt_k between two events is not the same for the corrected wheel speed signal (shown in red). When comparing the corrected wheel speed signal with the input signal, it can be seen that there is a vertical offset. This may be because a complete convergence of the estimated PWE with the prescribed PWE values is not obtained. The amplitude of 0.1 rad/s is retained in the corrected wheel speed signal. Also, a phase-lag can be observed in Figure 3.13 between the input and the corrected wheel speed signal. This is because, the corrected wheel speed in the event domain is computed using a backward difference technique, as shown in (3.23). Finally, PWE are estimated with an accuracy of 95% for the constant wheel speed case using the revolution based RLS estimator.

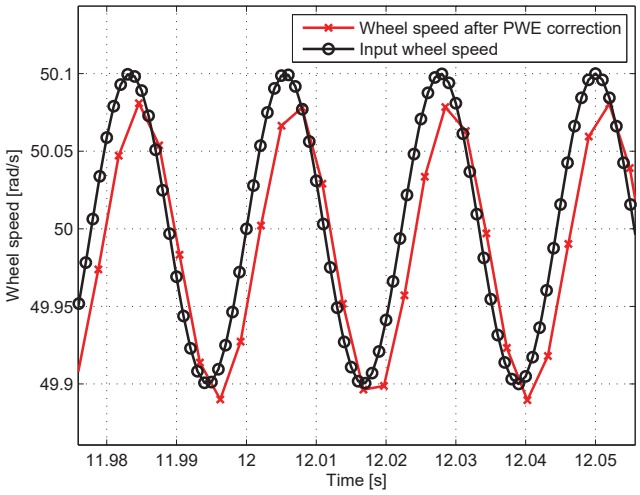

Figure 3.13: Comparison of input wheel speed and corrected wheel speed signal.

3.5 Summary

The ABS wheel speed sensor works on an event based sampling approach, which has been discussed in this chapter. The tooth in the sensor toothed wheel is not always ideal and they are subjected to irregularities, which is called pulse width errors(PWE). The PWE affects the accuracy of the wheel speed signal. A revolution based RLS estimator is discussed in this chapter, which is used to estimate the PWE of all the detected edges in one revolution. The revolution based RLS estimator is modelled with and without the constraint. The constraint in the estimator model is that the sum of all PWE in one revolution is considered to be zero. However, when implementing the constraint in the model, there is an overshoot in the covariance matrix value, which is a major drawback observed. Hence, the estimator is modelled without constraint for further evaluation in this thesis.

A constant wheel speed case is considered for evaluating the revolution based RLS estimator. In addition to this, an artificial set of PWE for 43 detected edges in the toothed wheel are introduced. The constant wheel speed is then event sampled with the influence of the prescribed PWE. The revolution based RLS estimator is then evaluated for this case. The prescribed PWE values for all detected edges are estimated with an accuracy of 95% after around 1900 revolutions of the sensor toothed wheel. The 95% accuracy is determined by computing the difference between the estimated and the assumed PWE values. The event based wheel speed signal is then corrected with the estimated PWE for all detected edges. Furthermore, the PWE attenuation in the wheel speed signal should also be observed when converting the wheel speed signal from the event domain to the time domain. This will be the next objective and is discussed in Chapter 4.

Chapter 4

Wheel Speed Signal Re-sampling

This chapter explains the method to convert the corrected wheel speed signal in the event domain to a wheel speed signal with a fixed sample period in the time domain. The data from test case 1 in section 3.4.2 is used in this chapter to evaluate the re-sampling technique and to analyse the frequency content of the wheel speed signal.

4.1 Re-sampling: event to time domain

Converting the wheel speed signal from the event domain to a wheel speed signal in the time domain is the next phase in this thesis. As already explained in Chapter 3, the time period between every event is not constant and hence, the objective here is to find a re-sampling method, to obtain the wheel speed signal with fixed sample period.

Motivation for re-sampling: The primary motivation for re-sampling is to convert the event based signal with varying time period to the time based signal with fixed sample period. This is in order identify the first tyre resonance frequency of the wheel speed signal in the time domain, as there is no accurate method to describe the frequency content of an event domain signal. The first tyre resonance frequency is further used for identifying the tyre-road friction. Hence, to perform this operation, certain requirements have to be satisfied and these are listed below:

- The re-sampling method should be applicable for real time purpose.
- The aliasing of frequencies above the Nyquist frequency in the wheel speed signal should be minimum.
- Complexity of the method should be low

Furthermore, to obtain a reliable wheel speed signal with a fixed sample period, the signal has to follow the criteria of the sampling theorem. The sampling theorem states that the continuous signal has to be sampled at a frequency greater than twice the Nyquist

frequency f_N. An aliasing effect occurs if the re-sampled wheel speed signal contains frequency components above the Nyquist frequency. In that case, the input frequency gets aliased below the Nyquist frequency, which ultimately causes an aliasing effect. The aliasing effect can be seen as sum and difference of the input signal frequencies with multiples of sampling frequency f_s.

In a normal time sampling, the sample period is constant and the aliasing effect can be reduced by using an anti-aliasing filter. An anti-aliasing filer is generally used as an input to the continuous signal before the sampling process [15]. This avoids unwanted higher frequencies above the Nyquist limit from being sampled. However, in the application of the ABS wheel speed sensor, the sample period is not constant since the signal is event based sampled and hence, a normal anti-aliasing filter cannot be used. Therefore, in order to comply with the sampling theorem, a higher sampling frequency f_s is fixed. This will minimize the aliasing effect, and ultimately convert the event based signal to the time based signal with fixed sample period. Furthermore, this replaces the function of an anti-aliasing filter. In this case for identification of the first tyre resonance frequency, it is desirable to have a reliable signal up to about 500 Hz such that sufficient information is available in the frequency content of the re-sampled wheel speed signal. For obtaining a reliable signal of up to 500 Hz, the event based wheel speed signal has to be sampled at a frequency f_s of 1000 Hz, i.e the fixed sample period Δt is 0.001 s. The sampling frequency f_s of 1000 Hz is selected based on the wheel speed and the frequency of the edge detection, which is further shown in Table 4.1. The frequency of edge detection f_k in one revolution is computed as shown by

$$f_k = \frac{\Omega_k N}{2\pi} \tag{4.1}$$

From (4.1), f_k is the frequency of the edge detection, i.e for either N=43 or 86, and Ω_k is the corrected wheel speed at every detected edge. Table 4.1 shows the frequency and time period of the edge detection for various constant wheel speeds. The wheel speed is assumed to be constant for one revolution without any influence of PWE. Hence, the wheel speed at each detected edge Ω_k is also constant, and the time period Δt_k for the detected edges can be computed according to (3.1). From Table 4.1, it can be seen that for a vehicle speed less than 90 km/h with 43 detected edges, the input frequencies of the detected edges are less than the Nyquist frequency, i.e 500 Hz. Similar case is observed for vehicle speed below 50 km/h with 86 detected edges. The input frequencies of the detected edges, which are above the Nyquist frequency can potentially be aliased back, however, this does not occur as signal components above 300 Hz are not expected due to limitations of the structure borne noise. The structure borne noise can be seen when a component transmits vibration to structures in contact with it. For frequencies above 300 Hz, only airborne noise occur for tyre-wheel systems. Moreover, the PWE or other disturbances might still exist above 500 Hz, but it is expected that the amplitude of the frequency components above 500 Hz after PWE compensation are negligibly small. Also from Table 4.1, it can be seen that an interpolation method has to be chosen in order to obtain a time signal with fixed sample period.

Table 4.1: Frequency and time period of the detected edges for various constant wheel speeds.

V [km/h]	V [m/s]	Ω [rad/s]	N=43 f_k [Hz]	N=43 Δt_k	N=86 f_k [Hz]	N=86 Δt_k
10	2.777	8.960	61.319	0.0163	122.638	0.0081
20	5.555	17.921	122.645	0.00815	245.290	00040
30	8.333	26.881	183.964	0.00543	367.928	0.0027
40	11.111	35.842	242.826	0.00407	490.581	0.0020
50	13.888	44.800	306.596	0.00326	613.192	0.0016
60	16.666	53.763	367.935	0.00271	735.871	0.0013
70	19.444	62.724	429.26	0.00232	858.523	0.0011
80	22.222	71.683	490.574	0.00203	981.148	0.0010
90	25	80.645	551.907	0.00181	1103.814	0.00090
100	27.777	89.603	613.212	0.00163	1226.425	0.00081

In the field of signal processing, many methods of interpolation exist [16]. As already described in Chapter 2, two methods are proposed in [7] and they are: Linear Interpolation and Kernel based interpolation. From that only the linear interpolation is considered in this thesis. The second method on kernel based approach is too complex and not fast enough for real time processing, and hence it is not considered for further implementation. The linear interpolation is further expanded by using a cubic polynomial interpolation and is explained in this thesis. Another interpolation method, which is considered is the integrated sampling method. The integrated sampling method is theoretically explained in [17]. Hence for this thesis work, two methods are considered from the previous work for converting the event domain to the time domain, which are: linear interpolation and integrated sampling. The inputs to the interpolation methods are Ω_k and t_k from the event domain and a fixed sample period Δt.

4.1.1 Piecewise Cubic Hermite Interpolating Polynomial (PCHIP)

One of the two methods from the previous work in [7] is the Linear Interpolation (LI). The resultant output in the interpolation technique is the re-sampled wheel speed signal with fixed sample period $\Omega_{p\Delta t}$ where, p is the number of the sample with fixed sample period Δt .

The linear interpolation constructs the resultant wheel speed signals in the time domain at the fixed time period Δt between the range of two known input samples from the event domain i.e t_k and Ωk. The interpolated time period should further satisfy the following criteria given in (4.3) in order to obtain the wheel speed signal in the time domain.

$$t_{k-1} < p\Delta t < t_k \tag{4.2}$$

The working of the piecewise linear interpolation is represented as

$$\Omega_{p\Delta t} = \Omega_{k-1} + (p\Delta t - t_{k-1})\frac{\Omega_k - \Omega_{k-1}}{t_k - t_{k-1}} \tag{4.3}$$

The resultant output from the linear interpolation is the re-sampled wheel speed signal with fixed sample period $\Omega_{p\Delta t}$. The obtained wheel speed signal $\Omega_{p\Delta t}$ is a continuous function of $p\Delta t$, however, the first derivative of $\Omega_{p\Delta t}$ is not continuous as the derivative is a constant value. Also, the relation between two samples cannot be concluded by just determining the slope using the LI method. Hence, a better way to expand the linear interpolation, and also to satisfy the interpolation method based on derivatives is obtained using a Piecewise Cubic Hermite Interpolating Polynomial (PCHIP). The cubic polynomial interpolation is performed using MATLAB function "PCHIP", and is used to determine the re-sampled wheel speed signal in the time domain. The "PCHIP" is also termed as shape-preserving cubic interpolation. A comparison between linear interpolation and piecewise cubic hermite interpolating polynomial is illustrated in Figure 4.1.

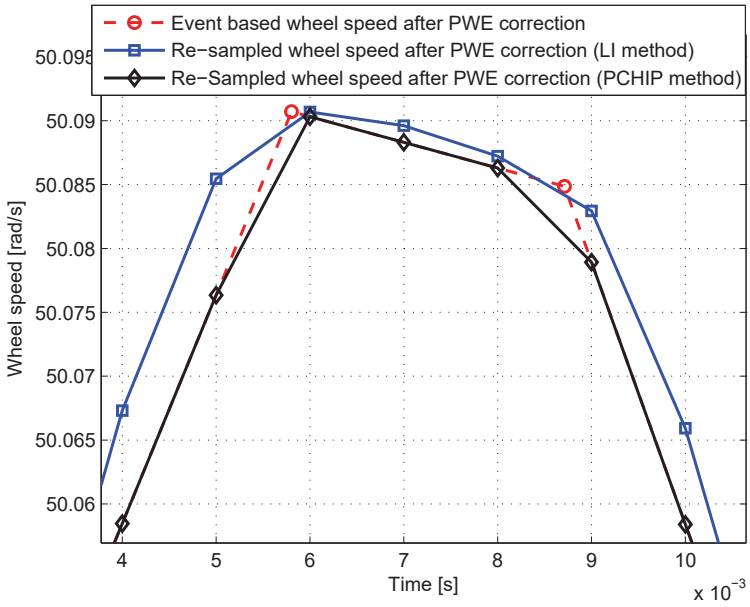

Figure 4.1: Conversion of event based corrected wheel speed signal with re-sampled wheel speed signal in the time domain using LI and PCHIP methods.

In Figure 4.1, the re-sampled wheel speed signal using LI and PCHIP can be seen with fixed sample period Δt. The input signal to the interpolation is the event sampled corrected wheel speed signal Ω_k, which can also be seen in Figure 4.1. The event based corrected wheel speed signal is considered from Section 3.4.2 of Chapter 3. In Figure 4.1, it can be observed that the values of the re-sampled wheel speed signal $\Omega_{p\Delta t}$ using PCHIP method is closer to the actual wheel speed values from the event domain Ω_k, when compared to

the re-sampled wheel speed signal values using LI method. Thus, the difference between the interpolated and the actual value is less when using PCHIP interpolation method. Moreover, if the number of events are more within the interpolated time period Δt or when the events are widely spaced, a higher order cubic polynomial interpolation is always preferable to use in order to obtain a smooth result of the wheel speed signal in the time domain. This can also be seen in Figure 4.1 as the varying time period Δt_k is larger than Δt. Hence, it can be concluded that the piecewise cubic hermite interpolating polynomial can be used for converting the event domain data to the time signal with fixed sample period.

4.1.2 Integrated Sampling (IS)

An alternative method to convert the event domain signal to the time domain signal is by integrating the corrected wheel speed signal over a fixed sample period Δt [17]. In general for a time varying continuous signal Ω_t, the integrated sampling method integrates the signal over the entire sample period Δt and is given by

$$\Omega_{p\Delta t} = \frac{1}{\Delta t} \int_{(p-1)\Delta t}^{p\Delta t} \Omega_t dt \tag{4.4}$$

The main advantage with this method is that the integral can be recovered exactly, when calculating the summation of the signal over time and it is represented in (4.5). The drawback of this method is that it gives a positive bias when the signal is decreasing and negative bias when the signal is increasing [17].

$$\int_0^{p\Delta t} \Omega_t dt = \sum_{p\Delta t} \Omega_{p\Delta t} \Delta t \tag{4.5}$$

This method works like an averaging technique as the continuous signal is integrated in every fixed sample period Δt. The averaging over the sample period also minimizes the aliasing effect in the signal [17].

Since, minimizing aliasing is one of the major requirements for re-sampling from the event to the time domain, the integrated sampling method is considered. Similarly as in (4.4), the same approach is used to convert the event domain signal to time signal with fixed sample period. The procedure to re-sample using IS method is described below with an example, and is illustrated in Figure 4.2.

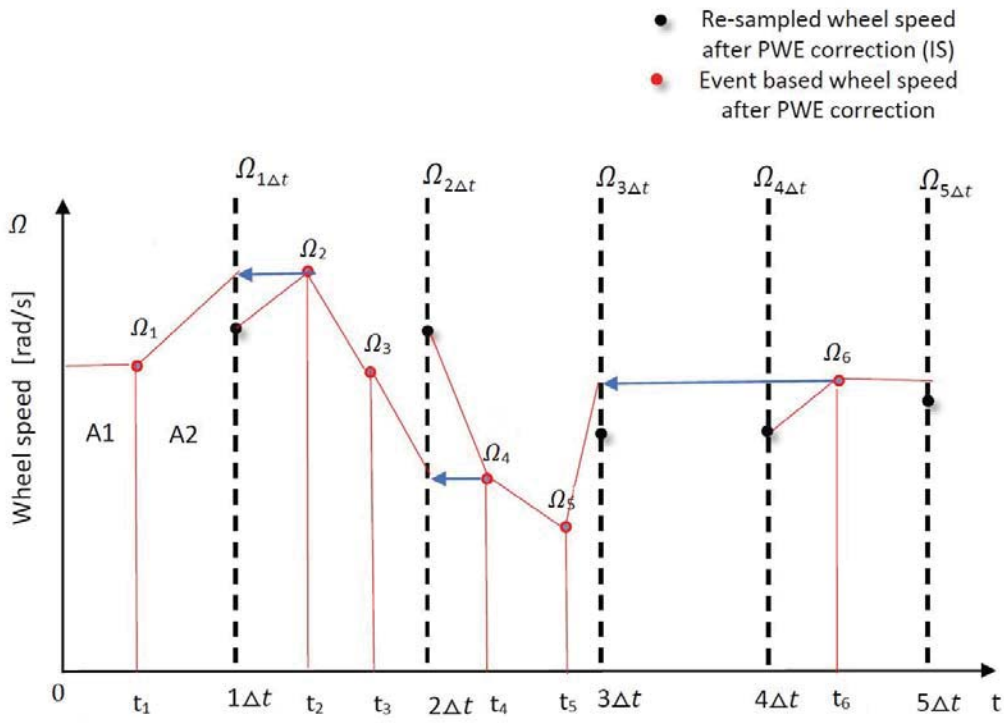

Figure 4.2: Procedure for re-sampling event domain signal to the time domain signal using IS method.

Figure 4.2 shows an example with six event based corrected wheel speed data Ω_k, which are represented as red dots. The re-sampled wheel speed signal $\Omega_{p\Delta t}$ using IS method is represented by black dot. Similar to the PCHIP method, a fixed sample period Δt is taken and the event based wheel speed signal is converted to a time signal at every Δt. For example, in Figure 4.2, between 0 and $1\Delta t$, the area A1 and A2 is computed. At fixed sample period $1\Delta t$, the re-sampled wheel speed $\Omega_{1\Delta t}$ is determined by dividing the sum of areas, A1 and A2 over the fixed sample period $1\Delta t$. This computation is given by (4.6). The re-sampled wheel speed $\Omega_{1\Delta t}$ is the average wheel speed for the first time period $1\Delta t$ and this is represented as a black dot in Figure 4.2.

$$\Omega_{1\Delta t} = \Omega_1 t_1 + [0.5(\Omega_1 + \Omega_2)(1\Delta t - t_1)] \tag{4.6}$$

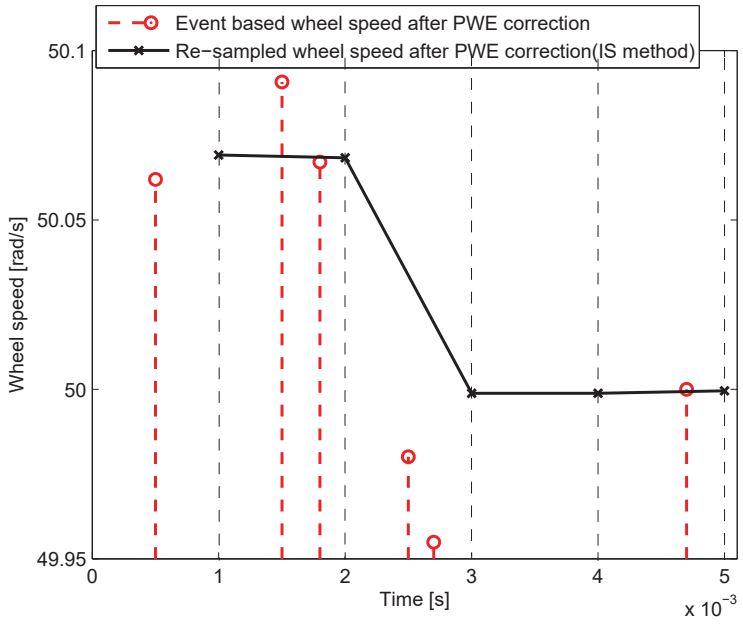

Figure 4.3: Conversion of event based corrected wheel speed signal with re-sampled wheel speed signal in the time domain using IS method.

From Figure 4.2, in the interval $[t_1,\ 1\Delta t]$, area A2 is computed by using the first event based corrected wheel speed value from the period $2\Delta t$, and this is illustrated as a blue line with arrow in Figure 4.2. This procedure is similar at other fixed time periods $p\Delta t$ and hence, the re-sampled wheel speed $\Omega_{p\Delta t}$ is obtained. From Figure 4.2, it can be seen that between $3\Delta t$ and $4\Delta t$, there are no events. Hence, in $4\Delta t$, the same re-sampled wheel speed value determined at $3\Delta t$ is taken.

An exampled to illustrate the IS method is shown in Figure 4.3. The IS method is evaluated using the same procedure as shown in Figure 4.2 to convert the wheel speed from the event domain to the time domain. In this example, the fixed sample period Δt is assumed to be 0.001 s and an average over every $p\Delta t$ is computed in order to obtain the re-sampled wheel speed signal $\Omega_{p\Delta t}$.

However, the IS method may be effective in reducing the aliasing effect only if there are more events in every Δt. As also observed in Figure 4.2, when there are no events, the same wheel speed value at the previous fixed sample period is taken and this might further induce a bias when the signal is increasing/decreasing [17]. In order to obtain more events within the fixed time period Δt, the varying sample period Δt_k from the event based signal should be much smaller than Δt.

To investigate the robustness of the integrated sampling method in the application of wheel speed sensor processing, time period for every detected edge Δt_k is computed. The

computation is tabulated in Table 4.1. From Table 4.1, it can also clearly be seen that the time period Δt_k for the constant wheel speeds up to 100 rad/s with 43 events are much higher than the assumed fixed sample period Δt (0.001 s or 1000 Hz). Thus, in most of the cases there are either one or no events in every fixed sample period Δt. The same is true for constant wheel speeds less than 80 rad/s with 86 events. Hence, this method gives bias in the re-sampled wheel speed signal and may not make any significant reduction in the aliasing effect.

Conclusions on the interpolation method Two different interpolation methods are chosen based on the requirements criteria in Section 4.1. The Piecewise Cubic Hermite Interpolating Polynomial(PCHIP) is simple to compute and also the aliasing effect is minimized as the wheel speed signal is sampled at higher sampling grequency f_s. The second method on integrated sampling is again computationally efficient, however not ideal for this application as this method is only applicable for cases when the number of events within the fixed time period Δt are higher. Hence, for further evaluation, only the piecewise cubic polynomial interpolation (PCHIP) is considered for converting the event based signal to time signal.

Results and analysis: Artificial test case 1 in the time domain

The results and analysis of the processing method for the artificial test case 1 from Section 3.4.2 is illustrated below.

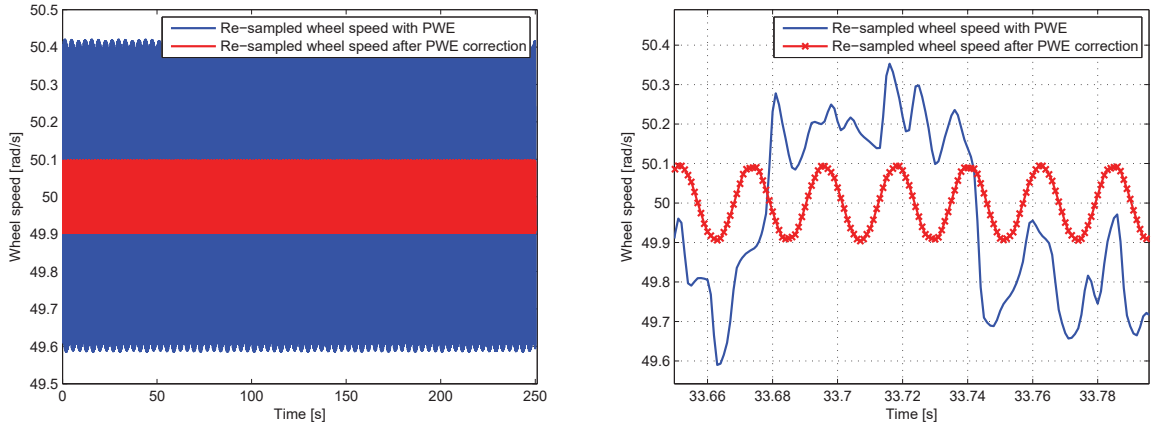

(a) (b)

Figure 4.4: (a) Comparison of re-sampled wheel speed signals before and after PWE correction (b) Zoomed-in image.

From Figure 4.4(a) it can be seen that the re-sampled wheel speed signal is obtained for every fixed sample period of 0.001 s using the PCHIP method. The re-sampled signal can be seen clearly in the zoomed-in image in Figure 4.4(b). The re-sampled wheel speed signal

can now be compared with the input wheel speed signal taken for the test case in Chapter 3, and the resultant plot is given in Figure 4.5.

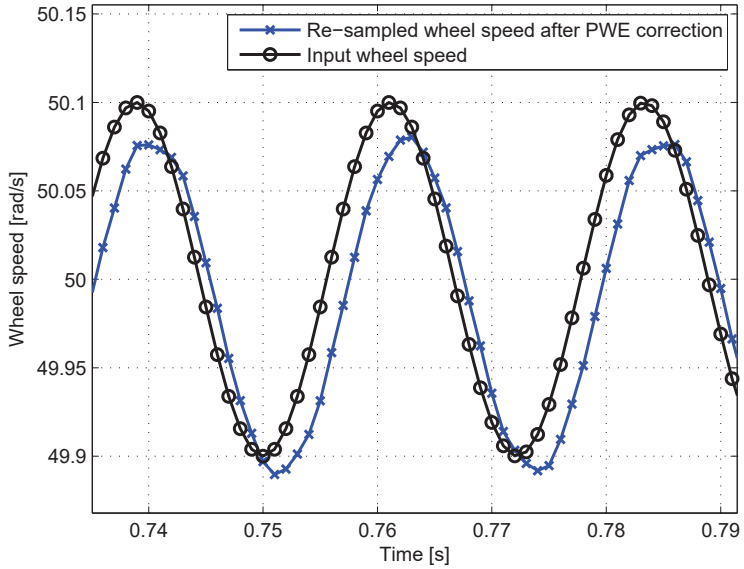

Figure 4.5: Comparison of the re-sampled wheel speed signal and the input wheel speed signal in the time domain.

Figure 4.5 shows the comparison of the re-sampled wheel speed signal with that of the input wheel speed signal without PWE. The input wheel speed signals is illustrated in Figure 3.9 (a). The comparison shown in Figure 4.5 shows similar results as in Figure 3.13. The re-sampled wheel speed signal can now be converted to frequency domain.

4.2 Spectral analysis of the wheel speed signal

In this thesis, the main objective is to estimate the first tyre resonance frequency by eliminating the pulse width errors from the wheel speed signal. If the resonance peak is seen at the desired frequency, without any influence of PWE harmonics, then the developed processing method can be used as part of a friction estimation method. Knowing the magnitude of the pulse width errors is by itself not important. However, the harmonics due to the PWE in the signals has to be attenuated to make the wheel speed signal suitable for the clear identification of first tyre resonance frequency. The occurrence of the harmonics due to PWE can be computed theoretically from the fundamental frequency. The fundamental frequency is computed as shown in (3.7). The amplitude of the harmonics depends on the magnitude of the PWE. An essential tool to check the frequency content in a wheel speed signal is using the power spectral density (PSD). Power spectral analysis

using the MATLAB function "pwelch" determines the frequency content of the re-sampled wheel speed signal with and without PWE.

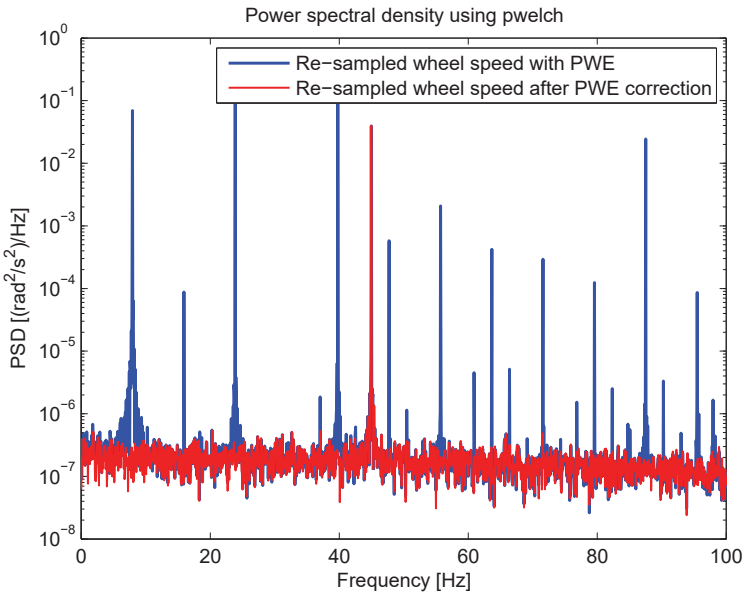

Figure 4.6: Power spectral density of the re-sampled wheel speed signal.

Figure 4.6 shows the Power spectral density of the re-sampled wheel speed signal before and after PWE correction. The re-sampled wheel speed signal with pulse width errors has both the signal component at 45 Hz together with other harmonics at different frequencies due to PWE. Hence, the signal component at 45 Hz could not be distinguished from the harmonics due to PWE.

Theoretically, the mean constant speed for this case is around 50 rad/s. When computing according to Equation (3.7), the fundamental frequency for the PWE is at 7.957 Hz and the subsequent harmonics of the PWE are the multiples of the fundamental frequency. From Figure 4.6, the fundamental frequency lies at 7.8 Hz for the re-sampled wheel speed signal with PWE and the corresponding harmonics for every PWE are seen as multiples of this fundamental frequency. Thus, the harmonics are clearly seen in the re-sampled wheel speed signal with PWE, which also approximately matches with the theoretical values.

However, after PWE correction, there is no signs of any harmonics due to PWE and the 45 Hz frequency can be clearly identified. Hence, it is concluded that the PWE estimation is effective in suppressing PWE harmonics. Furthermore, the re-sampling method with a sampling frequency f_s of 1000 Hz is effective enough to minimize aliasing, and also for converting the event domain data to the time domain.

4.3 Summary

In this chapter, re-sampling procedure is presented for converting the event domain signal with varying time period to the time domain signal with fixed sample period. A high fixed sample period $\Delta t = 0.001$ s is taken, considering the possibility to minimize the aliasing effect during re-sampling. Moreover, when working with an event based wheel speed signal, a normal anti-aliasing filter cannot be used.

Piecewise Cubic Hermite Interpolating Polynomial (PCHIP) approach is used to convert the event based wheel speed signal with varying time period to time based wheel speed signal with fixed sample period. In addition to the PCHIP method, an Integrated Sampling (IS) approach is also proposed in this chapter. However, it is concluded that the IS method is more suitable when there are more events in every fixed sample period Δt.

The constant wheel speed case from Section 3.4.2 is considered in this chapter for evaluating the processing method in the time domain phase. When the re-sampled wheel speed obtained from the PCHIP method is transformed to frequency domain, a clear identification of 45 Hz signal component is observed without any disturbances due to PWE errors. In concluding, the developed processing method is completely validated for the constant wheel speed case.

Chapter 5

Validation of the Wheel Speed Signal Processing Method

In this chapter, different driving conditions are evaluated to get an insight on the robustness of the developed wheel speed processing method. Also, the chapter gives details to identify the operating conditions in which the developed method could actually work in real life. For this chapter, two different wheel speed test cases with the same PWE are implemented.

5.1 Simulation model description

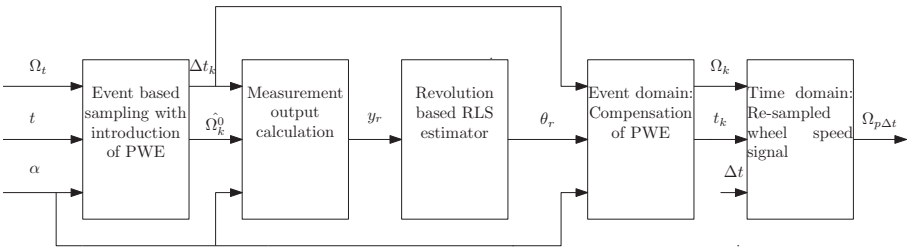

Figure 5.1: Block diagram of the simulation model.

Figure 5.1 represents the block diagram of the simulation model for validating the artificial test cases. The input to the simulation model is the wheel speed time signal, without any influence of PWE and, the angle α. In the event based sampling block, the input wheel speed signal Ω_t with respect to time is first converted to angular distance and then the artificial PWE values are event based sampled, according to (3.21). The outputs of the event based sampling block are the time period for every detected edge Δt_k and the reference wheel speed $\hat{\Omega}_k^0$. Then the measurement output y_k is computed from the angle α, known values of reference wheel speed $\hat{\Omega}_k^0$, and the time period Δt_k for every detected edge, which is based on (3.16). Since, the RLS estimator determines PWE for all detected

edges in one revolution, the measurement output for one revolution y_r is taken into the revolution based RLS estimator. The output from the revolution based RLS estimator block is the PWE estimate for all edges after one revolution, and is represented by θ_r in Figure 5.1. In the event domain block, the corrected wheel speed signal for every detected edge Ω_k is obtained by compensating with estimated PWE. The correction of the wheel speed is performed as given by (3.23). Next, the corrected wheel speed signal Ω_k w.r.t time instants t_k is taken as inputs to the time domain block. The inputs together with a fixed sample period Δt is interpolated using the PCHIP method in order to obtain the re-sampled wheel speed $\Omega_{p\Delta t}$.

5.2 Model testing with artificial test cases

In the previous test case as explained in Chapters 3 and 4, a constant wheel speed with a sinusoidal disturbances is evaluated. It is also shown that the 45 Hz frequency component in the signal is also observed in the PSD plot of the wheel speed signal without any harmonics due to PWE. Hence, in this section, the processing method is tested with respect to varying wheel speed and some normal driving conditions. This is further to prove the robustness of the developed wheel speed signal processing method.

Artificial test case 2: Varying wheel speed

In this test case, the wheel speed is artificially assumed to be varying from an initial value of 50 rad/s to 80 rad/s, which is illustrated in Figure 5.2(a) and the angular distance profile is shown in Figure 5.2(b).

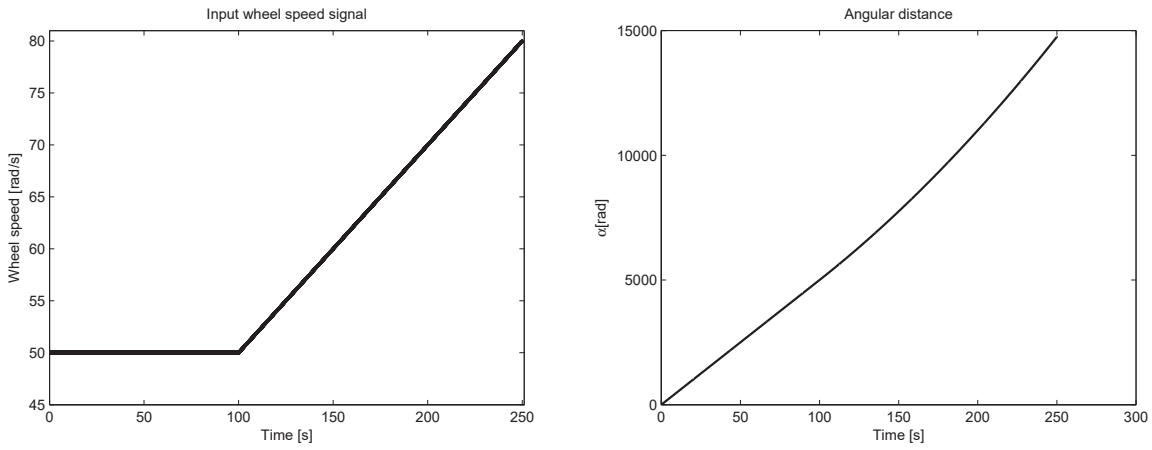

(a) (b)

Figure 5.2: (a)Wheel speed signal (b)Angular distance signal.

The wheel speed is initially constant and after 100 s it increases linearly to 80 rad/s in 150 s.

A signal component, $s(t) = 0.1sin(2\pi ft)$ with frequency of $f = 45$ Hz is introduced to the varying wheel speed. The total time for this test case is 250 s, which is similar to test case 1. The total number of teeth L =43 and the number of detected edges N_{edge} per tooth is 1. The values of the PWE are the same as the one, taken in test case 1, and a similar procedure of event based sampling is followed to include the PWE into the angular distance signal.

Results and analysis

According to the block diagram of the simulation model in Figure 5.1, the first part after collecting the required event based data is to estimate the PWE in the event domain. Hence, after collecting the inputs to the estimator, the revolution based RLS estimator is evaluated for this test case. The resultant PWE estimates for this test case are shown in Figure 5.3(a) and (b).

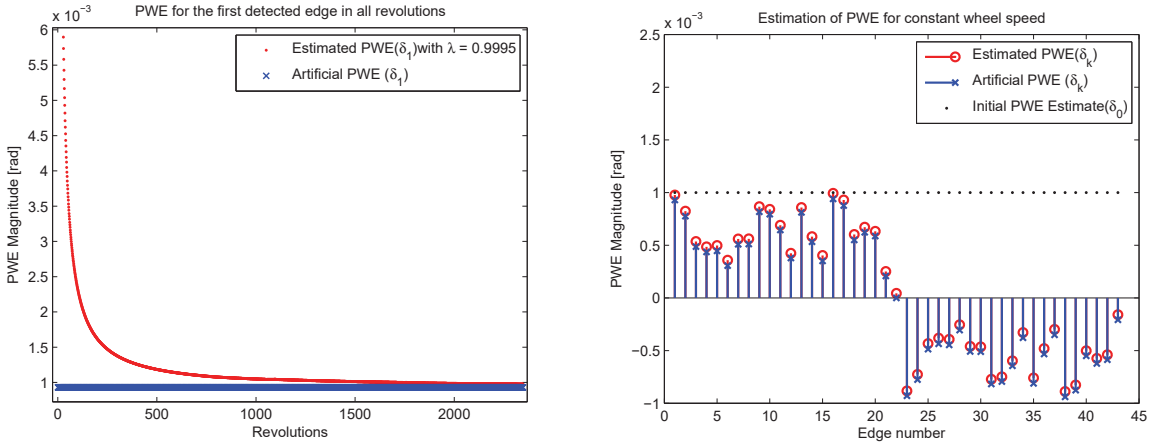

(a) (b)

Figure 5.3: (a)Convergence of estimated and the artificial pulse width errors for the first detected edge in all revolutions (b)Estimation of pulse width errors for all detected edges.

Figure 5.3(a) shows the PWE estimate for the first detected edge δ_1. The PWE estimate for the first detected edge converges to the prescribed PWE values initially taken in the estimator. Furthermore, the convergence of the estimated PWE is obtained with an accuracy of over 95%. Similar to the constant wheel speed case, the PWE estimate is checked at various revolutions and, it is concluded that the convergence happens slowly. However, after 1950 revolutions, an accuracy of 95% can be obtained. Also similar to test case 1, a minimum of 550 revolutions is necessary for a reasonably accuracy of 80% for the PWE estimate. In this application, the final estimated PWE for all detected edges is logged at the end of the simulation, which is at the 2347th revolution and is also shown in Figure 5.3(b). Moreover, from test cases 1 and 2, it can be concluded that the one revolution delay in the reference wheel speed does not affect the PWE estimate, since a sinusoidal

disturbance is assumed. Hence, more realistic cases have to be considered in order to analyse the influence of the reference wheel speed in varying wheel speed conditions. Now since the PWE is estimated, the wheel speed is compensated for the errors according to (3.23). The computed wheel speed with and without PWE influence is shown in Figure 5.4(a) and (b).

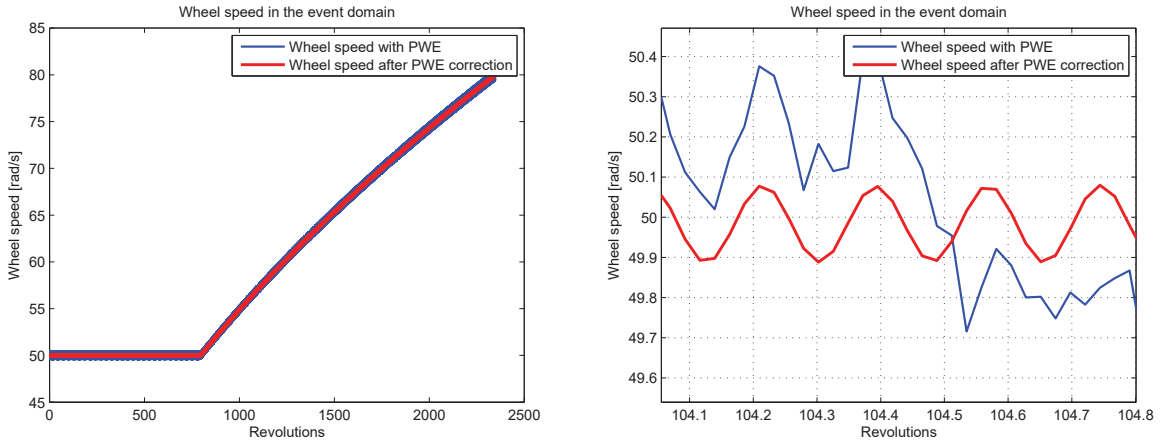

(a) (b)

Figure 5.4: (a)Wheel speed in the event domain before and after PWE correction for the entire revolutions (b)Zoomed-in image.

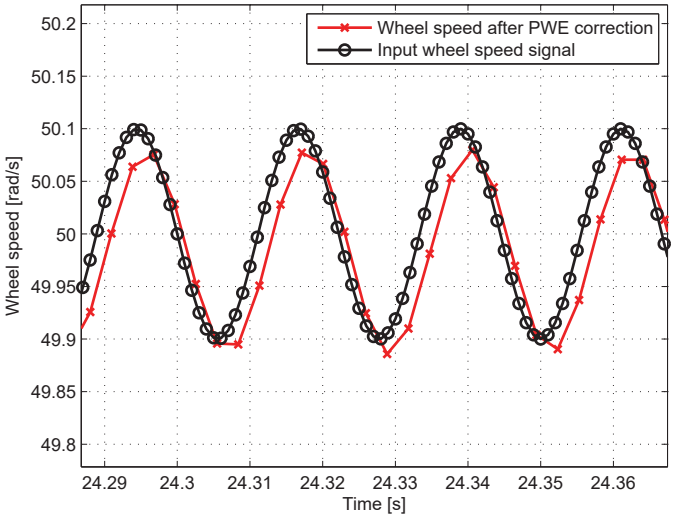

Figure 5.5: Comparison of input wheel speed and the event based corrected wheel speed signal.

From Figure 5.4(a), event based wheel speed signal before and after PWE correction for the entire revolutions of the toothed wheel can be observed. A zoomed in image is shown in Figure 5.4(b). Thus the corrected event based signal is compared with that of the input wheel speed signal and this is shown in Figure 5.5.

When comparing the event based corrected wheel speed signal with the input signal, it can be seen that there is a vertical offset. The vertical offset is mainly because the estimated PWE does not completely converge with the artificial PWE values that are introduced. Also, a phase-lag can be observed in Figure 5.5 between the input and the corrected wheel speed signal. This is because, the corrected wheel speed in the event domain is computed using a backward difference technique, as shown in (3.23).

The event based wheel speed data with varying time period Ω_k is now converted to time based wheel speed signal $\Omega_{p\Delta t}$ with fixed sample period. The conversion to time domain is done using the piecewise cubic hermite interpolating polynomial (PCHIP) method as explained in Chapter 4 and, the fixed sample period Δt is assumed to be 0.001 s (f_s= 1000 Hz). The quality of the re-sampling can be further assessed by analysing the frequency content of the wheel speed signal. The major requirement is that the corrected wheel speed signal should not contain harmonics due to PWE. The PSD plot of the re-sampled wheel speed signal before and after PWE correction is shown in Figure 5.6.

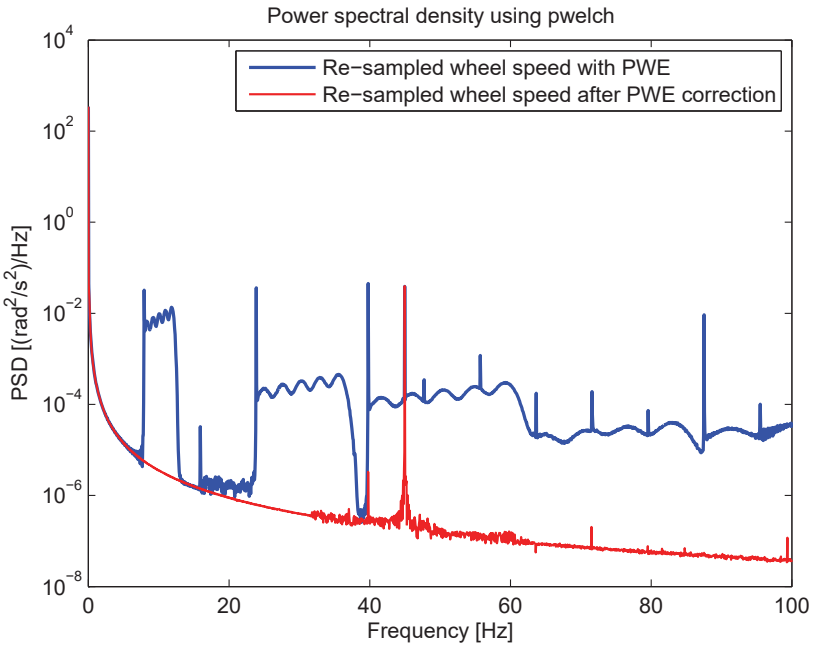

Figure 5.6: Power spectral density of the re-sampled wheel speed signal.

From the PSD plot shown in Figure 5.6, it can be seen that the re-sampled wheel speed

signal after PWE correction is free from harmonics due to PWE. For varying wheel speed, the PWE disturbances are more widely spread across the frequency range, which can also be seen in the PSD plot for the wheel speed signal with PWE. The resonance of 45 Hz in the signal component is observed in both wheel speed signals before and after PWE correction. From test cases 1 and 2, it can be concluded that an accuracy of 95% for the estimated PWE can be achieved for constant and slowly varying wheel speed conditions. However, these two cases are evaluated only with sinusoidal disturbances.

Artificial test case 3: Normal driving condition

In this test case, a more realistic time history for the wheel speed signal is considered. The values of the wheel speed signal are taken from the vehicle CAN data, when the vehicle is driven in the city. The wheel speed signal from the CAN data is low pass filtered, which is why it does not show any high frequency content. The CAN data for the wheel speed signal is shown in Figure 5.7(a) and the angular distance profile is shown in Figure 5.7(b). Here again, the same PWE as in the test cases 1 and 2 is taken and the wheel speed is event based sampled according to the Equation 3.21. Since, high frequency components cannot be obtained from the CAN signal, a signal component, $s(t) = 0.1sin(2\pi ft)$ is added to wheel speed signal with frequency of 45 Hz to mimic the first-tyre resonance. The resultant PWE estimate is shown in Figure 5.8(a) and (b).

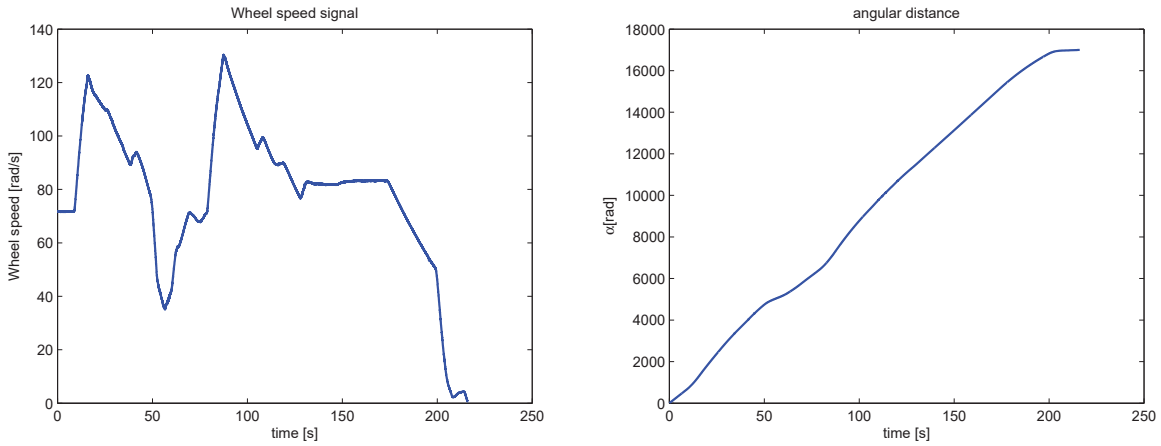

(a) (b)

Figure 5.7: (a)Wheel speed signal (b)Angular distance signal.

Results and analysis

In Figure 5.8(a), the convergence of the PWE can be seen for the first detected edge from the initial estimate to final value. However, from Figure 5.8(a), it can also be seen that at certain revolution, the estimate of PWE does not decrease monotonically. This

is because the vehicle is braking at many places and the wheel speed signal is reduced drastically. The braking areas and a steep increase/decrease in vehicle acceleration can be seen from Figure 5.7(a). The quality of the reference wheel speed signal $\hat{\Omega}_k^0$ is very low at the braking areas and also in certain acceleration maneuvers. Moreover, this is due to the bias in the reference wheel speed computation. The assumption of one revolution delay, is inaccurate during these conditions. The measurement output based on (3.16) is affected when the reference wheel speed is inaccurate. The measurement output further affects the estimation error, which ultimately makes the PWE estimate to decrease non-monotonically. The convergence of the PWE happens very slowly, hence, the estimator adapts quickly when there is a constant wheel speed driving soon after a braking or acceleration. Also in this case, the estimated PWE starts to adapt to the decreasing trend after around 2000 revolutions. This is due to a constant wheel speed driving between 2000 and 2500 revolutions and this can be seen seen in Figure 5.9(a). Hence, the final PWE estimate in this case is logged during the constant wheel speed condition i.e at the 2500th revolution. Similar to the test cases 1 and 2, the accuracy of the estimated PWE to the prescribed values are around 95% for all the detected edges. The wheel speed signals in the event domain is shown in Figure 5.9 before and after PWE correction.

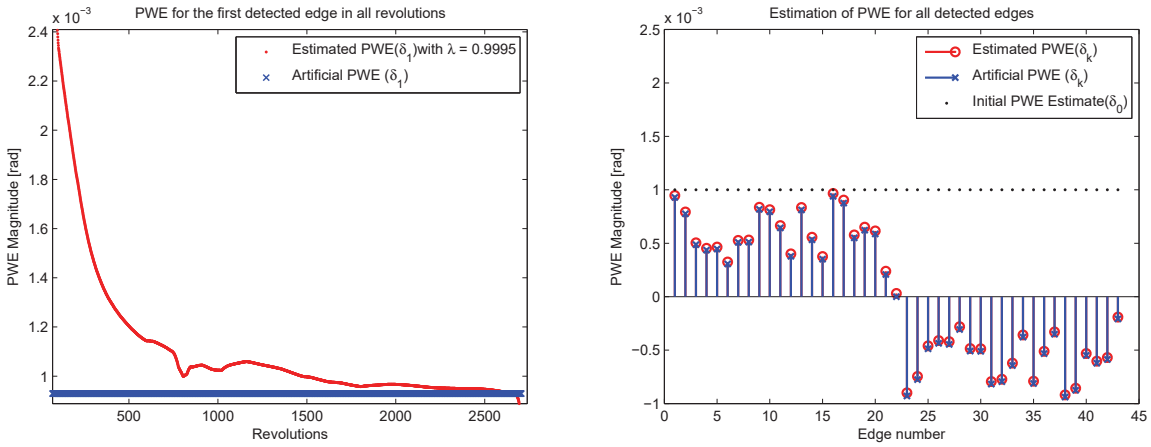

(a) (b)

Figure 5.8: (a)Convergence of estimated and the artificial pulse width errors for the first detected edge in all revolutions (b)Estimation of pulse width errors for all detected edges.

From Figure 5.9(a) and (b), it can be seen that the quality of the wheel speed signal is improved after correcting the signal with PWE. Since the model is evaluated off-line, the PWE estimate are logged at 2500th revolution, i.e during constant wheel speed driving. The logged value at the 2500th revolution are used for correcting the entire wheel speed signal in off-line. This is because the PWE does not change over time, and a maximum of 95% accuracy for PWE estimate is also obtained at the 2500th revolution. The zoomed in image of the wheel speed signals in the event domain are shown in Figure 5.9(b). The

resultant event based data are converted to a time based wheel speed signal and the PSD of the re-sampled wheel speed signal before and after PWE correction is shown in Figure 5.10.

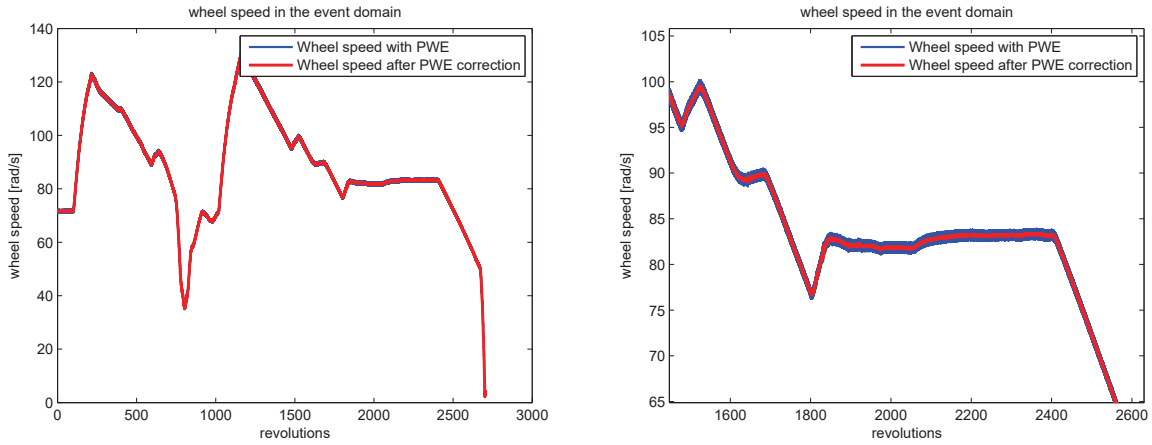

(a) (b)

Figure 5.9: (a)Wheel speed in the event domain before and after PWE (b)Zoomed-in image of the wheel speed in the event domain.

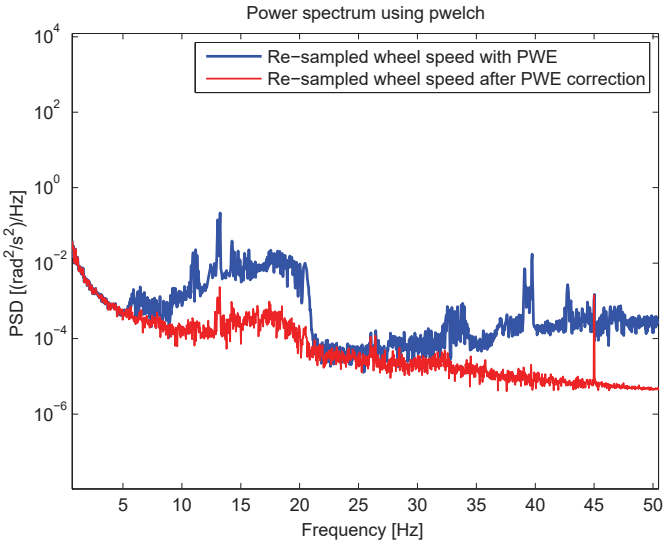

Figure 5.10: Power spectral density of the re-sampled wheel speed signal.

The power spectral density of the re-sampled wheel speed signal can be seen in Figure 5.10. Since the wheel speed signal is varying over time, the harmonics due to PWE are distributed

over the entire frequency range. The 45 Hz signal component cannot be distinguished from the PWE harmonics in the re-sampled wheel speed signal with PWE. However after PWE correction, harmonics due to the PWE is suppressed and the resonance frequency at 45 Hz is visible in re-sampled wheel speed signal.

5.3 Summary

In this Chapter, two test cases are discussed for the developed processing method: varying wheel speed with sinusoidal disturbances and a realistic wheel speed case from the vehicle CAN data. For specific test cases in the simulation environment, a 95% accuracy for the estimated PWE is obtained from the revolution based RLS estimator after 1900 revolutions. In a more real driving conditions, as shown in test case 3, it is always recommended to log the PWE estimate in a constant speed driving scenario. This is because the reference wheel speed computation with one revolution delay is reasonably accurate during constant wheel speed. Also from test case 3, it can be observed that the PWE estimate is not monotonically decreasing when the vehicle is braking or maneuvering. The logged PWE estimate during the constant wheel speed driving can be used in the correction for various wheel speeds, which is also clear from the test case 3. The test case results also shows that the signal component introduced with 45 Hz frequency is clearly visible in the PSD plot of the wheel speed signal without any disturbance due to PWE. Hence, the objective for this thesis work is achieved in the simulation environment. In the next chapter, the developed wheel speed sensor processing method will be evaluated with the real world data.

Note: The estimated PWE results for all detected edges are also evaluated after about 560 revolutions, where an accuracy of 80% is achieved. The 80% accuracy also proves to be reasonably accurate in eliminating the PWE and a clear frequency component of 45 Hz is seen. This case is explained in Appendix A.

Chapter 6

Application to Vehicle Measurement Data

This chapter explains the processing of the the wheel speed sensor signal for vehicle measurements. It is important to verify whether the pulse width error estimation works well in real life and it is also necessary to show that the first tyre resonance frequency can be obtained without any disturbances due to PWE. The measurement data is used to get a better view of how the system could work in reality.

6.1 Experimental set-up

In this application, the ABS sensor consists of a toothed wheel with 43 teeth and the processing electronics detects two edges i.e the rising and falling edge for every tooth. Having information for both rising and falling edges of the teeth, increases the resolution of the wheel speed signal and thus, this is an improvement compared to the sensor detecting either only the falling or rising edges. The number of detected edges depends on the vehicle speed. When the vehicle is moving slowly, the number of tooth edges detected will be less and when the vehicle speed is high, the number of detected edges will increase. The computation of the frequency of edge detection is already explained in Section 4.1 of Chapter 4.

The theory behind the working principle of the ABS sensor is already mentioned in Chapter 3, however it is necessary to know how the raw data is collected for real time applications in order to implement the developed processing method. The data collection from the ABS wheel speed sensor for the real data application is carried out using a dSPACE auto box. Usually the raw data from the ABS sensor is guided to an ECU unit, pre-processed and transmitted through a CAN unit. In this case, since the processing of the wheel speed signal is actually dealt with, the raw wheel speed data from the ABS sensors are captured by a special electrical circuit such that the data is also available for the dSPACE auto box. The dSPACE auto box that is used in this application is the DS4002 Timing and Digital I/0 Board.

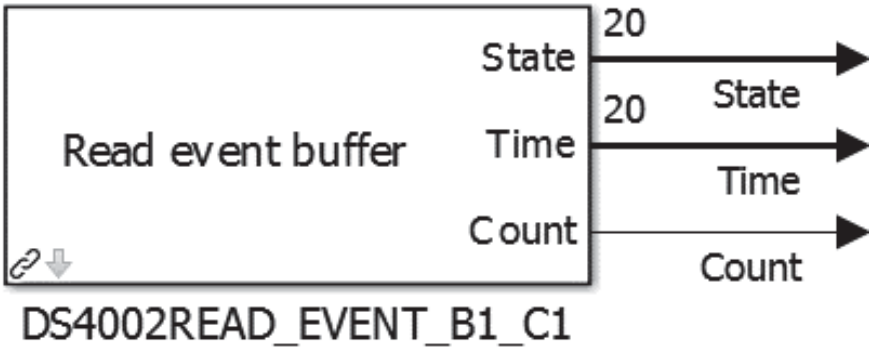

Figure 6.1: dSPACE block to read access to the event buffer.

The raw data values from dSPACE are directly transmitted to Simulink for further processing through a Simulink dSPACE block. The Simulink real time dSPACE block outputs the number of detected edges of the teeth and the corresponding time instants during a sample time of 0.01 s. Hence, after each sample (100 Hz or 0.01 s), the raw event based data from the dSPACE block is provided in a vector format to the Simulink model. However, the size of the vector, which provides the edge detection states and times should be pre-defined. The maximum wheel speed that can be logged without missing any detected edges is determined by the number of elements in the vector. For this purpose, the maximum vector size is set to 20. This fixing of the vector size allows a maximum vehicle speed of 165 km/h, which is beyond the normal driving conditions and, is also sufficient for the experiments. The raw data stored in vector format of the dSPACE block is represented in Figure 6.1. From Figure 6.1, it can be seen that the bock consists of three components: state, time and count. The Simulink output for the dSPACE block is listed in Table 6.1.

Table 6.1: Relation of dSPACE to Simulink output

dSPACE Output Port	Simulink Output
State (output 1)	-1....1 -1: No edge detected 0: Falling edge detected 1: Rising edge detected
Time (output 2)	0....2^{30}200 ns (214.75 s)
Count (output 3)	0...511

The state in the dSPACE block outputs either 1 or 0 at each event, which indicates the detection of rising or falling edge of the tooth from the sensor toothed wheel. If no edge is detected, the state outputs -1. The count provides the total number of edges passed after every sample time of 0.01 s. The time in the dSPACE block gives the value of the time

instants for each detected edge and the resolution of the time vector is 200 ns. If no edges are detected, time sets value 0 in the time vector. As the minimum difference between two time instants is 200 ns, the maximum counter value that can be stored is limited to 511. Hence, when the time output port reaches a maximum value of $2^{30}200$ ns (214.75 s), the time instants values starts counting again from 0. The maximum value for a 32 bit signed integer is represented as $(2^{31}-1)$. For the application of the ABS wheel speed sensor with two detected edges in each tooth, the maximum value of 214.75 s is obtained by $\frac{(2^{31}-1)200e^{-9}}{2}$

Test vehicle description: The test vehicle is a Volkswagen Jetta 2.0 TSI DSG Highline and it is a front wheel drive car with ABS and Traction control. The test vehicle is shown in Figure 6.2. The vehicle is equipped with several sensors and these are:

- An ABS sensor, which is used to provide the wheel speed signal. This is the only sensor used in this research and there is one ABS sensor in all four wheels. The toothed wheel in this ABS sensor has 43 teeth.

Figure 6.2: Test vehicle for the friction estimation project at TNO.

- An Inertial Measurement Unit (IMU) to provide longitudinal, lateral acceleration, GPS position and yaw velocity of the vehicle.
- A steering wheel angle sensor.
- A non-contact optical velocity measuring sensor (CORRYS) is used for the accurate measurement of vehicle speed, both in the longitudinal and lateral direction.

- An intelligent tyre (ityre), using piezo accelerometers, is mounted at the rear left (RL) wheel of the vehicle and its data is logged at 4000 Hz.

  During the testing at the proving grounds, measurement data for the entire vehicle is logged with a dSPACE at 1000 Hz sampling frequency. During separate measurements for the ityre, data is logged at 4000 Hz sampling frequency. The reason for this is that the data acquisition system has insufficient capabilities to log all signals simultaneously at 4000 Hz. Hence, two different measurement data sets are available from testing.

Test track description: The aim of the experiment is to collect data from test track and to process the wheel speed sensor signals. The measurement data used in this research are obtained from testing the vehicle at "Automotive Testing Papenburg" in Germany. The tests that are done at the high speed oval test track (ORK) at ATP are used for the validation of the processing method developed in this research. Data is selected from the available measurement sets in which the vehicle is driven in a normal driving conditions over a long distance. The high speed oval test track is shown in Figure 6.3.

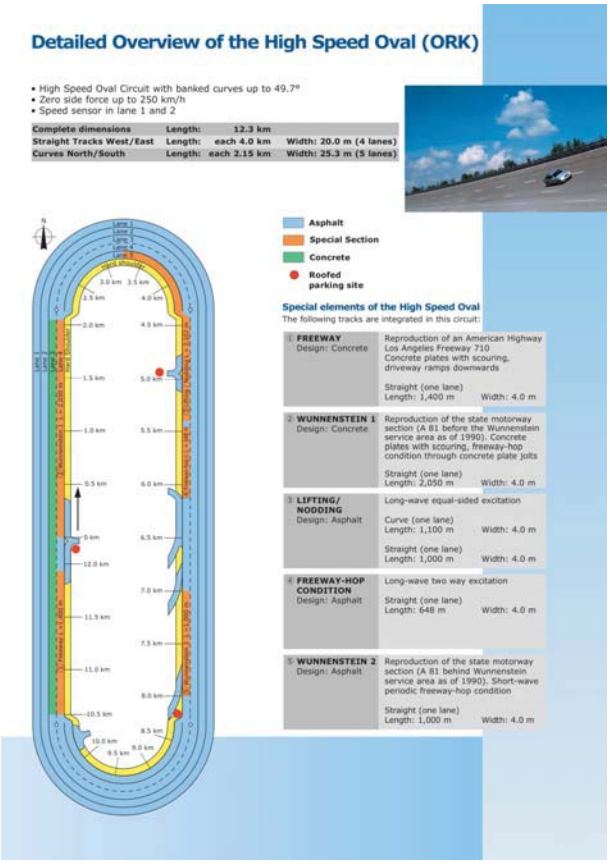

Figure 6.3: Test track at ATP.

6.2 Measurement replay model

The measurement replay model is very similar to the simulation model given in Figure 5.1. The measurement replay model is where the vehicle measurement data collected from testing, are being used as inputs, giving the advantage of being able to test the developed processing method off-line. An off-line approach is considered in this research as it serves as an important tool in rapidly developing a prototype of the algorithm for real-time implementation. The implementation of the measurement replay model is presented as block diagram in Figure 6.4.

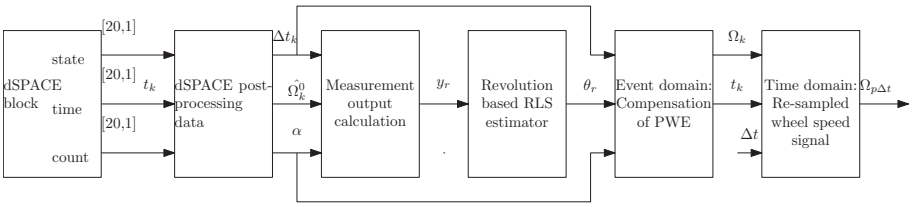

Figure 6.4: Block diagram of the measurement replay model.

From Figure 6.4, the real data inputs from the ABS sensor are stored in the dSPACE block, which is already explained in Section 6.1. In the dSPACE post-processing data block, the raw data from the dSPACE are collected and the corresponding computation of the reference wheel speed and time period are done. However, before computing the time period and reference wheel speed, the values stored in the state and time vectors of the dSPACE for non detected edges are removed in this post processing block. After collecting the time period and reference wheel speed for each event, the measurement output y_k is computed. Since, the RLS estimator determines PWE for all detected edges in one revolution, the measurement output for one revolution y_r is taken in the revolution based RLS estimator. The output from the revolution based RLS estimator block is the PWE for all edges after one revolution, and is represented by θ_r. The inputs to the event domain block are the time period Δt_k and angle α. In the event domain block, the compensation of PWE in the event based wheel speed signal is done according to (3.23). The outputs from the event domain block are the corrected wheel speed Ω_k w.r.t time instants t_k in the event domain. The corrected wheel speed signal in the event domain is converted to a time based wheel speed signal with fixed sample period Δt, and this is performed in the time domain block. The resultant output from the time domain block is the re-sampled wheel speed signal $\Omega_{p\Delta t}$.

Proposed methods for measurement cases

In chapters 3 and 4, various methods to process the wheel speed signal are evaluated with test cases. The proposed methods for validating with vehicle measurement data are summarized below.

- **Estimation of pulse width errors in the event domain**: From Chapter 3, the proposed revolution based RLS algorithm is used for estimating PWE.
- **Conversion of event to time domain**: In Chapter 4, two interpolation methods are discussed and Piecewise Cubic Hermite Interpolating Polynomial (PCHIP) is selected for the testing. This method is selected for the measurement cases in this chapter due to its robust nature and also for its simple implementation. Two interpolation sample rates of 1000 and 4000 Hz are chosen in order to avoid the aliasing of signal components from higher frequencies. As already mentioned in Section 6.1, the test vehicle is equipped with an intelligent tyre (ityre) only on the rear left (RL) wheel and all the data for this tyre are logged at 4000 Hz separately. Since other signals from the ityre are sampled at 4000 Hz, the wheel speed signal after PWE correction is also time sampled at 4000 Hz. Hence, an interpolation sample rate of 4000 Hz is chosen for ityre measurement sets and 1000 Hz for vehicle measurement data set.

6.3 Model testing with measurement cases

6.3.1 Evaluation criteria

To evaluate the performance of the wheel speed sensor processing, the tests have to meet certain criteria. These criteria are as follows:

- Normal driving conditions should be considered i.e low acceleration, because the first-tyre resonance that is identified has to be used for estimating friction in these conditions. This is actually the main motivation for developing a wheel speed signal processing method.
- The test data should have a constant wheel speed driving section in order to log the PWE such that the logged PWE can be used for all driving conditions.
- The vehicle tests should be long enough such that a sufficient number of revolutions of the toothed wheel is obtained, i.e a minimum of 550 revolutions for 80% and 1950 revolutions for 95% accuracy.

6.3.2 Test scenarios

From the available measurement data sets for the ityre and the entire vehicle, 12 suitable measurement cases are selected, which satisfy the assumed evaluation criteria. From the 12 selected measurement cases, two cases are chosen in this section in order to explain the developed wheel speed signal processing method. These cases are presented in the Scenario 1 and Scenario 2 of this section.

Table 6.2: Design parameters of the RLS estimator

Parameter	**Values**
Forgetting factor (λ)	0.9995
Initial estimate (θ_0)	10^{-3}
Initial covariance (P_0)	I_{86}

Scenario 1: Constant wheel speed

The measurement data for this scenario is taken from the ityre measurement set and the test vehicle is driven with a speed of 80 km/h, and cruise control engaged at the ORK test track. There are special elements in the ORK track and this case belongs to the "second special element" as shown in Figure 6.3. This special element in the test track consists of a long-wave symmetric excitation. The wheel speed can be approximately computed by assuming a tyre radius R=0.31 m and the wheel speed is around 71.6 rad/s. The raw data from the dSPACE block is taken into the Simulink measurement replay model as shown in Figure 6.4 and an off-line analysis to process the wheel speed signal is carried out.

Results and analysis: As per the block diagram shown in Figure 6.1, the raw wheel speed data is collected from the dSPACE, and the next part in the processing of the wheel speed sensor signal is the estimation of pulse width errors in the event domain. The design parameters used for the revolution based RLS estimation are given in Table 6.2 and these are the same as the one used for the Simulation environment described in Chapter 3.

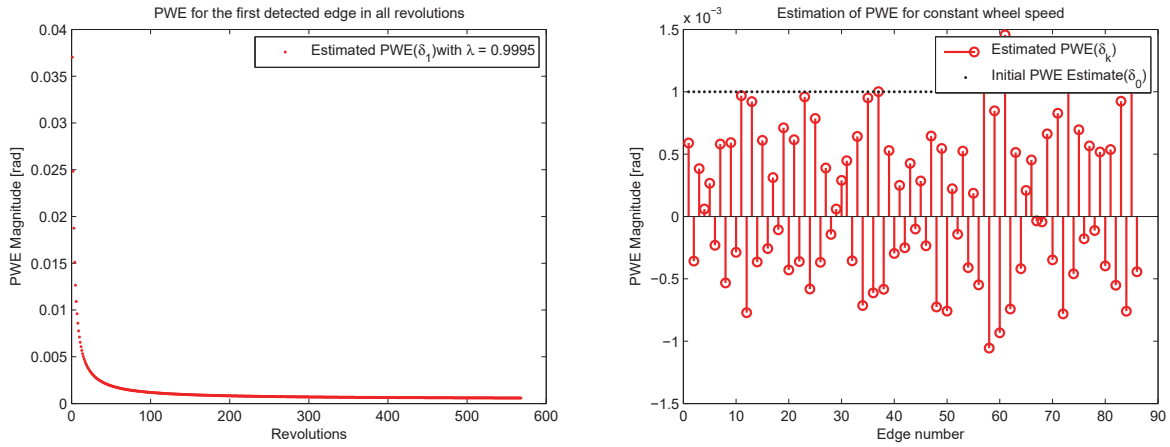

(a) (b)

Figure 6.5: (a)Convergence of the estimated and the artificial pulse width errors for the first detected edge in all revolutions (b)Estimation of pulse width errors for all detection edge.

Figure 6.5 shows the estimation of pulse width errors in the event domain. Figure 6.5(a) shows the convergence of the pulse width error for the first detected edge. Since an off-line approach is used for testing, the final values for all the 86 detected after 570th revolution are fixed and the PWE is shown in Figure 6.5(b). The next step is to compensate the wheel speed signal with the obtained PWE for all detected edges and this is shown in Figure 6.6(a) and (b).

In Figure 6.6(a), the wheel speed signal before (shown in black) and after PWE correction (shown in red) can be clearly seen. The PWE is compensated in the raw wheel speed signal from the dSPACE block and now the PWE free wheel speed signal is obtained. Figure 6.6(b) shows a detailed view on the impact of PWE in the wheel speed signal before and after PWE correction. The wheel speed signal after PWE correction (shown in red) is plotted above the wheel speed signal with PWE (shown in black) in order to show the influence of PWE in the signal.

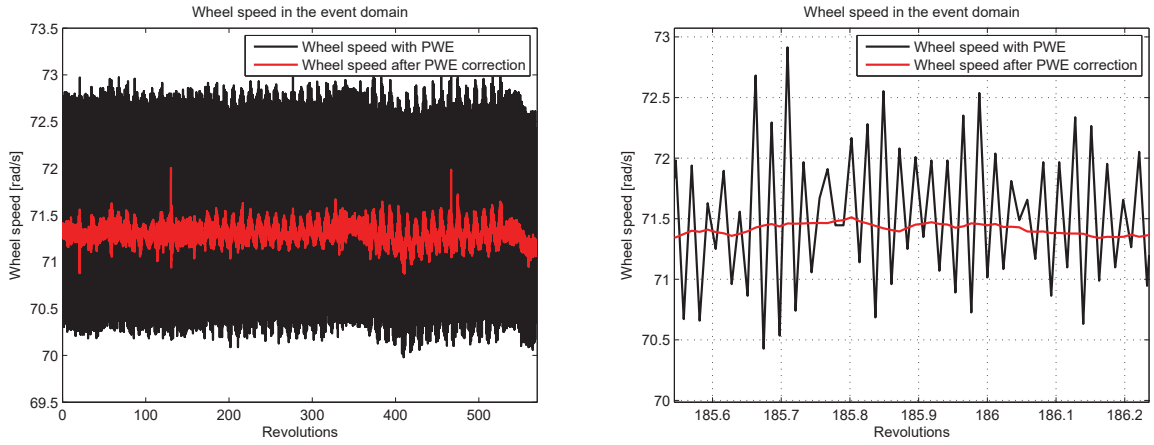

(a) (b)

Figure 6.6: (a)Wheel speed in the event domain before and after PWE (b)Zoomed-in image of the wheel speed in the event domain.

The next phase is to convert the event domain data to the time domain data. The piecewise cubic hermite interpolating polynomial method with a fixed sampling frequency f_s of 4000 Hz is implemented to the corrected wheel speed signal in order to obtain the re-sampled wheel speed signal in the time domain.

The PWE compensation and conversion to the time domain from the event domain data are not the only phases that are more important. One of the main requirements is to show that the harmonics due to PWE are attenuated in the power spectral density of the re-sampled wheel speed signal. Also the aliasing when re-sampling to time domain should be minimized. The power spectral density of the wheel speed signal is presented in Figure

6.7.

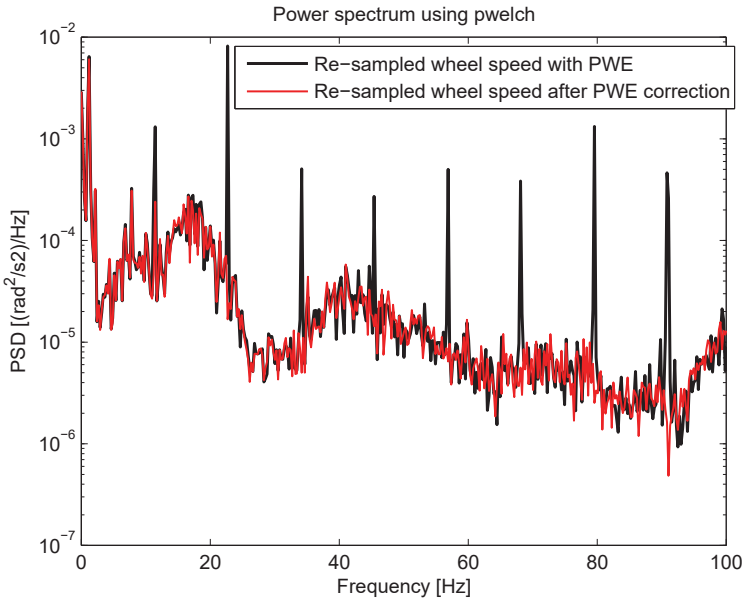

Figure 6.7: Power spectral density of the re-sampled wheel speed signal.

Figure 6.7 shows the power spectral density of the wheel speed signal before and after PWE correction upto 100 Hz. In the re-sampled wheel speed signal after PWE correction, between 0 and 10 Hz, the vehicle body or the sprung mass excitation can be observed and the natural frequency of the sprung mass is around 1.2 Hz. Similarly, the unsprung mass excitation is observed at around 16.6 Hz and the first tyre resonance can be identified at around 41 Hz. The harmonics due to PWE can be seen in re-sampled wheel speed signal with PWE (shown in black). In the re-sampled wheel speed signal with PWE, the first tyre resonance frequency could not be identified as the harmonics due to PWE has clearly higher energy peaks. The frequency at which the harmonics occur can be computed according to fundamental frequency shown in (3.6). In this case, since the wheel speed is constant and known to be around 71.6 rad/s, the fundamental frequency should be at 11.4 Hz. Other harmonics should be the multiples of the fundamental frequency. In Figure 6.7, it can observed that the first harmonic is at 11.5 Hz and multiples of the fundamental frequency are seen as different harmonics spread across 100 Hz. The frequency values at which the harmonics occur are similar to the theoretical values, which could conclude that the harmonics are mainly due to PWE. However, after suppressing the PWE harmonics, the first tyre resonance at 41 Hz can be identified in the re-sampled signal. Thus, it can be concluded that the developed processing of the wheel speed signal has been able to identify the first tyre resonance frequency without any influence of PWE for this case.

As the wheel speed processing method is working for this case, it is possible to determine

the estimated damping ratio and resonance frequency using a friction estimator. The friction estimator, which has already been developed at TNO, is combined with the developed processing method and is also explained in Section 1.1.

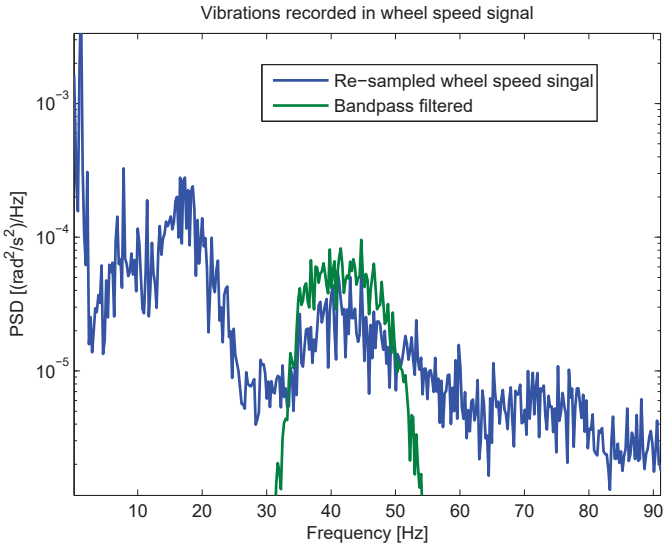

Figure 6.8: Power spectral density of the re-sampled wheel speed signal before and after band-pas filtering.

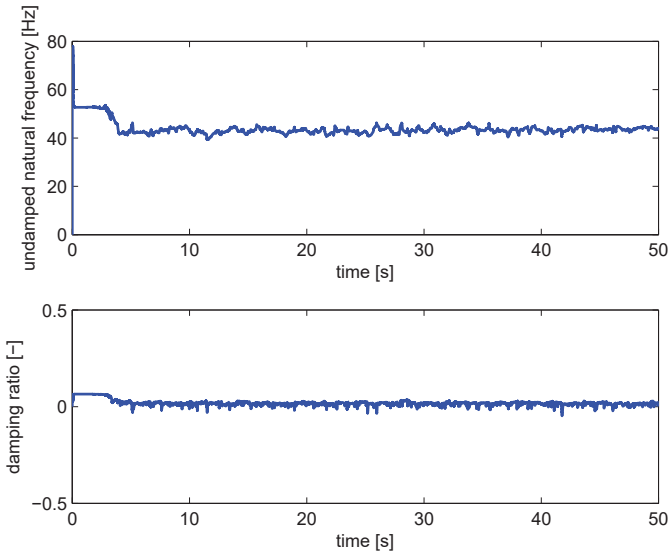

Figure 6.9: Estimated resonance frequency and damping ratio.

The main motivation behind the processing of the wheel speed signal is to estimate friction from the first tyre resonance frequency and damping, which can be possible from the measurement cases as well. Here, the re-sampled wheel speed signal from the measurement data after PWE correction is taken as input to the friction estimator model. The friction estimation is performed using an instrument variable (IV) estimation algorithm. The working of the IV algorithm is explained in [3] and the model is also taken from [3]. The PSD of the wheel speed signal is plotted in blue and is shown in Figure 6.8 along with the band pass filtered of the same wheel speed signal. The signal is band passed in the interval [30,50] Hz with a fourth order Butterworth filter. The output from the friction estimator model i.e the undamped estimated resonance frequency and the damping ratio are shown in Figure 6.9.

The damping ratio values are a measure for identifying the tyre-road friction coefficient through the longitudinal slip stiffness. As already explained in Section 1.1, the damping ratio decreases when the friction increases. From Figure 6.9, it can be seen that the mean value of the damping ratio is around 0.099 [-] and the resonance frequency is around 42.3 Hz. Furthermore, the resonance frequency estimated is not really the same as the first tyre resonance identified. This is caused by the tendency of the estimator to find the maximum of the signal in the middle of the bandpass frequency interval. Hence, further improvements in the estimation of resonance is required.

Scenario 2: Varying wheel speed

The input data for this scenario is taken from the vehicle measurement set, where the data logging for the ityre does not take place. The measurement data is logged when driving the vehicle from Helmond to Deurne. The measurement data is available for all the four wheels.

Results and analysis: Similar to Scenario 1, the estimation of PWE in the event domain comprehends the first part in the processing and the results of the estimation for 86 detected edges in this test case is shown in Figure 6.10.

As already mentioned, the raw data used from the entire vehicle measurement set consists of data for all four wheels. Hence, the PWE is also estimated separately for all four wheels. The PWE estimate shown in Figure 6.10 is logged at the 1950th revolution. With the obtained estimate of PWE, the raw wheel speed data in event domain is corrected for the entire run in all four wheels and this is shown in Figure 6.11.

Figure 6.11 shows that the vehicle is driven with varying speed and also at a normal driving conditions. This is in order to check the robustness of the developed processing method in real life conditions and also to check the behaviour of the PWE estimate at different driving conditions.

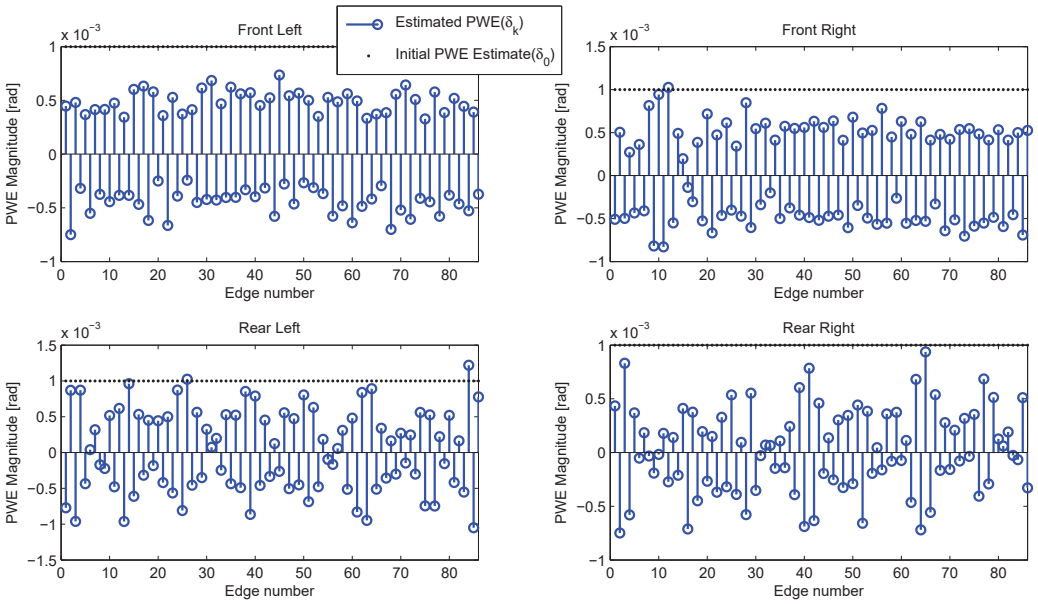

Figure 6.10: PWE estimate for all four wheels of the vehicle.

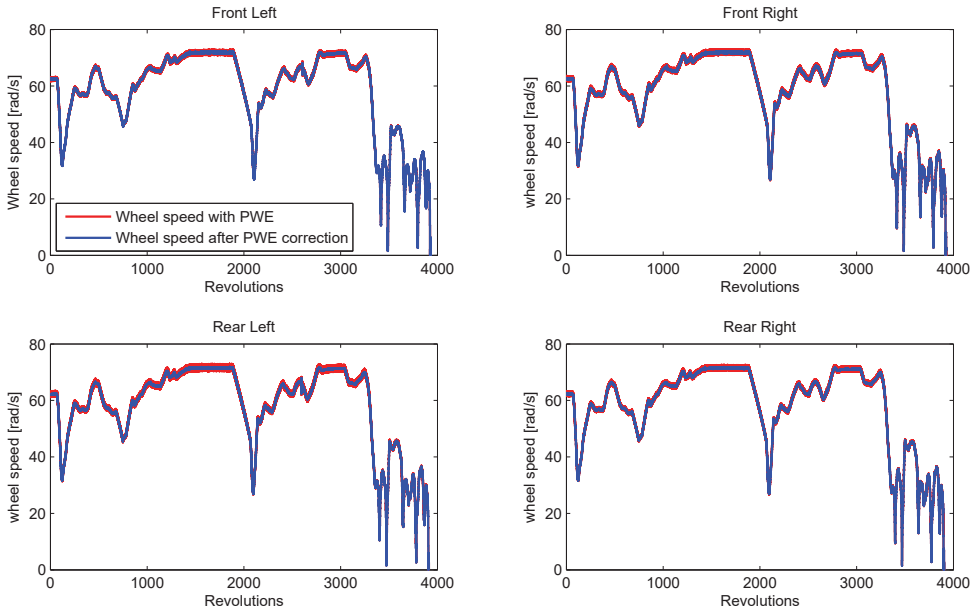

Figure 6.11: Wheel speed signal in the event domain before and after PWE correction for all four wheels of the vehicle.

There are several areas where the vehicle is braking and cruising, and hence, PWE estimate in these areas does not follow a monotonic trend. This is already mentioned in Chapter 5. However in this case, between 1450 to 1950 revolutions, a constant wheel speed can be seen, which is shown in Figure 6.12. The PWE estimate adapts well in this range as it follows a slow decreasing trend. Hence, the PWE estimate for all detected edges at the 1950th revolution are stored in the memory. This stored values are further used for correcting the entire wheel speed signal in an off-line condition.

From Figure 6.11, the wheel speed signal after PWE correction (shown in blue) can be clearly compared with that of the raw wheel speed signal with PWE (shown in red). A zoomed-in image of the wheel speed signal in the event domain is shown in Figure 6.12. The wheel speed signal is re-sampled from the event to the time domain using the Piecewise Cubic Hermite Interpolating Polynomial method (PCHIP). The power spectral density of the re-sampled wheel speed signal is represented in Figure 6.13.

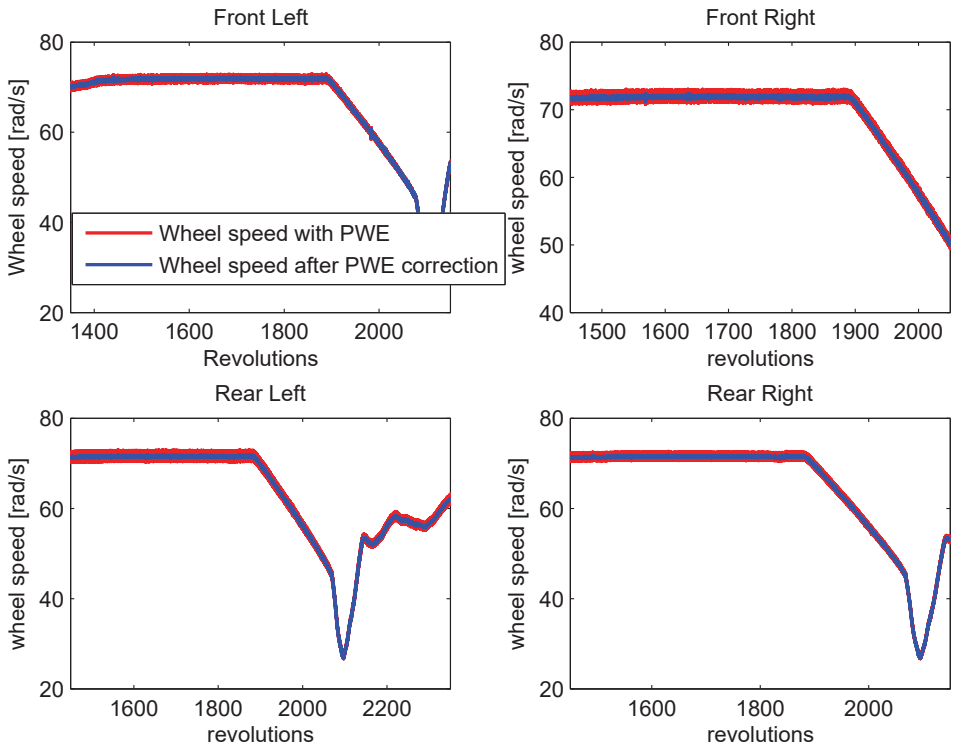

Figure 6.12: Zoomed-in image of the wheel speed signal in the event domain.

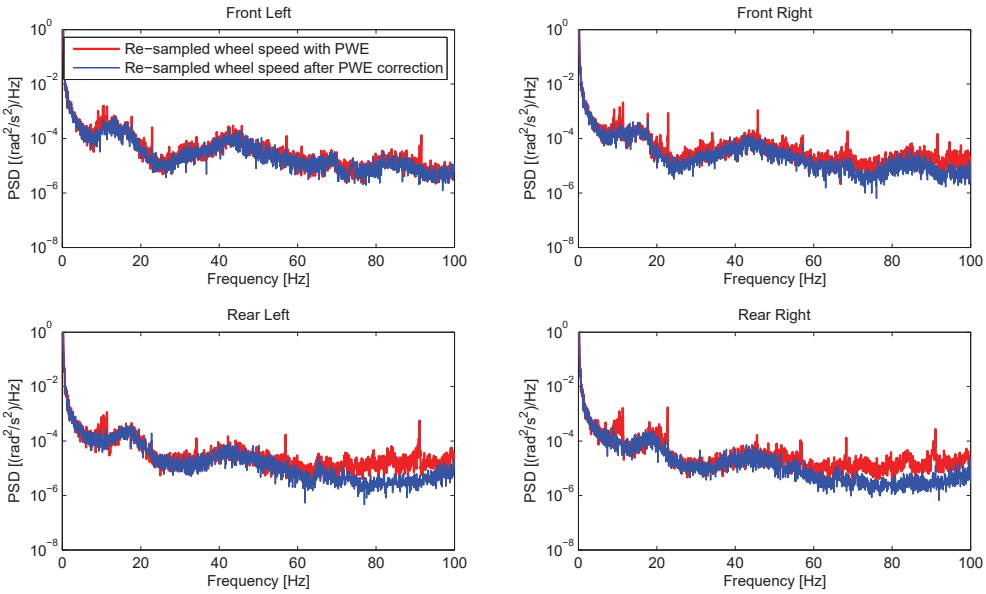

Figure 6.13: Power spectral density of the re-sampled wheel speed signal.

Figure 6.13 shows the power spectral density plot for all four wheels of the vehicle. Since the wheel speed is continuously varying, the harmonics due to PWE are distributed over the entire region in the frequency domain. On a closer look into the PSD plot of the re-sampled wheel speed signals after PWE correction, it can be observed that the first-tyre resonance for the front and real wheels are different. The first tyre resonance frequency without any harmonics due to PWE can be observed at around 42 Hz in the front wheels and around 43 Hz in the rear wheels. The front and rear wheels generally have difference tyre resonance as the front wheels are also affected by resonances due to the drive line. This is because, the drive line natural frequency can be observed below 100 Hz in the frequency content of the wheel speed signals.

6.3.3 Cross-correlation analysis of the PWE estimate

Since the exact position of each detected edge in the ABS sensor is not known, the relation between the PWE estimate obtained are not the same. This can be observed from different measurement cases. For example, the PWE estimate at each detected edge for the Rear Left wheel obtained from Scenario 1 are not the same as the one obtained in Scenario 2. In other words, the first edge that is detected will become the edge number 1, as the location of the edges are unknown at the start of every measurement data. Hence, a cross - correlation function is used in order to find the similarity of the PWE estimate with one case relative to other cases. For this reason, the value of PWE from Scenario 1 is considered as the base line and the value of PWE obtained for the other 8 cases are cross-correlated relative to this. Since more measurement data are available only for the ityre, the cross-correlation of

the PWE estimate is only performed for the Rear Left wheel in this thesis. This is further illustrated in Figure 6.14. In Figure 6.14, it can be seen that the PWE estimate for all 86 detected edges from different measurement cases are shifted based on the base line and the range of the PWE estimate for each detected edge can be computed by taking the mean value, which is further shown in Figure 6.15.

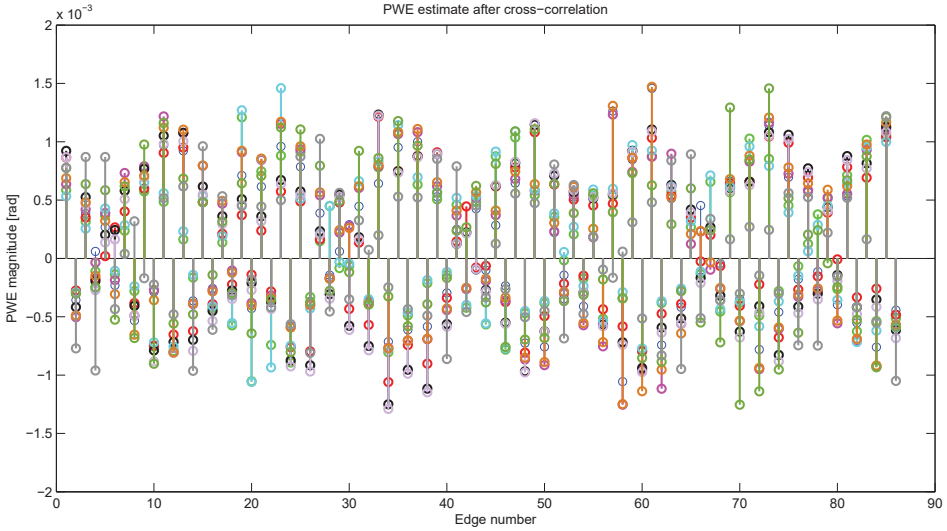

Figure 6.14: Shifted PWE estimate using the cross-correlation function.

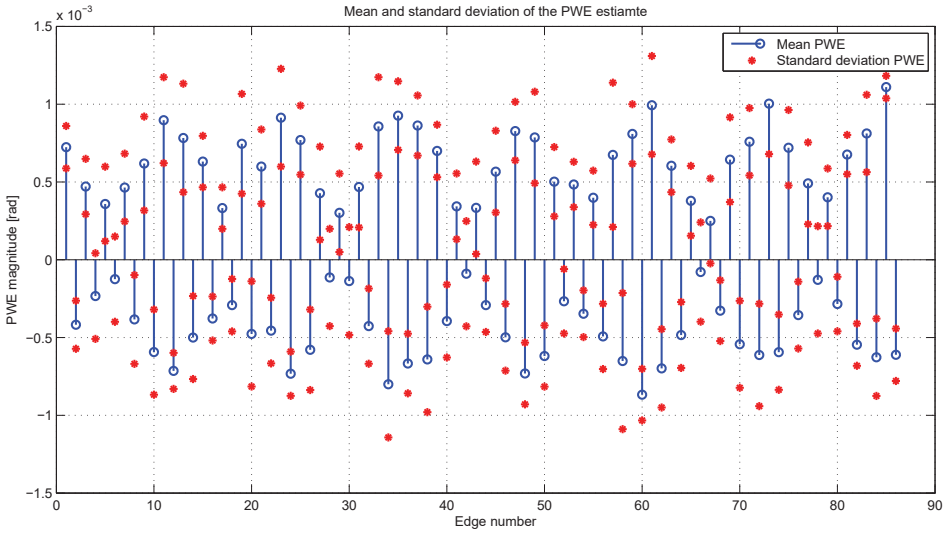

Figure 6.15: Mean PWE values for every detected edge.

The mean values computed for every detected edge are likely the real PWE estimate values for the ABS sensor in the Rear Left wheel. The standard deviation for the estimated PWE for all 86 detected edges are also presented in Figure 6.15. The accuracy of the PWE estimate for each detected edge can be concluded from the standard deviation value. If the first standard deviation is more widely spread from the mean value, then the accuracy of the PWE estimate is lower. If it is narrowly spaced, then the accuracy is higher. The average absolute value of the PWE for the ABS sensor in the Rear Left wheel is 8.8e-05 rad.

6.4 Summary

In this chapter, the developed processing method is evaluated for the vehicle measurement data. Two vehicle measurement cases are presented in this chapter: a constant wheel speed case from the iTyre measurement set and a varying wheel speed case from the vehicle measurement set. The wheel speed signal from the vehicle measurement data contains PWE and the revolution based RLS estimator is able to estimate the PWE and correct the raw wheel speed signal with the estimated errors. For the constant wheel speed set, the vehicle is driven at around 80 km/h. A first tyre resonance frequency is identified at 41 Hz from re-sampled wheel speed signal in the Rear Left wheel of the vehicle.

For varying wheel speed case from the vehicle measurement set, raw data are available for all four wheels. In this case, there are several areas where the vehicle is braking and hence, PWE estimate does not follow a monotonically decreasing trend. This is due to the bias in the reference wheel speed computation when the wheel speed is varying. However, in this case, the wheel speed is constant at a certain range. Hence, the PWE for all the detected edges are stored at the particular revolution in this range. Since the PWE does not change over time, the stored value of the PWE at the particular revolution, is to correct the entire wheel speed signal in this case.

Since an exact location of each detected edge is unknown at the start of the measurement, the relation between the PWE estimate from different measurement cases are not the same. Hence, a cross-correlation analysis is performed in order to yield the maximum relation between the PWE estimate. The average absolute value of the PWE in the Rear Left wheel from the iTyre measurement case is about 8.8e-05 rad.

Chapter 7

Conclusions and Recommendations

7.1 Conclusions

The goal of this master thesis is to develop a method to process the ABS wheel speed sensor signal, which guarantees that the wheel speed signal contains sufficient high frequency content for estimating the first tyre resonance frequency and damping ratio. This estimation of resonance frequency is an important factor for friction estimation under normal driving conditions. The thesis contains an extensive review of the sensor signal processing steps, which includes identification of pulse width errors in event domain and conversion of the corrected wheel speed signal from the event to the time domain.

For the first part in the processing step, an adaptive revolution based recursive least squares estimator for estimating the pulse width errors in the event domain is implemented in Chapter 3. The pulse width errors is estimated at each detected edge of the toothed wheel for one complete revolution and the raw wheel speed data in the event domain is compensated with such errors. The estimator is initially evaluated in the simulation environment with artificial values for constant and varying wheel speed. The results shows that the estimated values converges with the artificial values of the pulse width errors with an accuracy of 95 % after 1950 revolutions. However, the accuracy of the estimate in varying wheel speed condition is highly dependent on the computation of reference wheel speed. For this purpose, in this thesis, the final estimate of the PWE is always taken during the constant wheel speed conditions.

Two re-sampling methods are proposed in Chapter 4 to convert the corrected wheel speed data from event to time domain. The most straight forward approach of Piecewise Cubic Hermite Interpolating Polynomial (PCHIP) is used in this thesis in order to satisfy the targeted vehicle application, which requires real-time operation. Further, the re-sampled wheel speed signal is obtained minimizing aliasing as much as possible in the signal. The aliasing effect is reduced by using a higher sampling frequency as an anti-aliasing filter cannot be used for the event sampled data. From the power spectral density of the wheel

speed signal, it is concluded that the influence of PWE is attenuated and that it may be possible to identify the first tyre resonance frequency.

Finally, the developed method for wheel speed sensor processing is evaluated with vehicle measurement data obtained from tests performed at the ATP test track in Germany. The developed processing method is evaluated for test data from constant speed testing and the results shows that the quality of the wheel speed signal is improved by the PWE correction. This is also observed in the power spectral density of the wheel speed signal, where the first tyre resonance frequency is identified without any disturbances due to PWE. Furthermore, the developed processing method is also validated for measurement data obtained from normal city driving conditions and, here again the method is found to work reasonably well.

7.2 Recommendations

The developed processing method results in reasonably accurate processing of the wheel speed signal, if it is tested in an off-line condition. However there are many challenges related to successful implementation in real time conditions, which provides opportunities for further research.

In Chapter 3, it is concluded that the constraints in the PWE estimation is still a challenge to be implemented in the model. Hence, further research in implementing the constraints recursively has to be done.

Another aspect that can be improved in the estimation of PWE is to determine a more accurate way of computing the reference wheel speed. For real time implementation, the revolution based RLS estimator can also be turned off during braking or acceleration maneuvers.

It is highly recommended to cross-check the re-sampled wheel speed signal from the ABS wheel speed sensor with other high precision external speed sensor.

It is also recommended to conduct more tests under normal driving conditions for a longer time in order to further evaluate the developed processing method.

It is recommended to implement a method that could accurately determine the position of the edges in the toothed wheel i.e to give the accurate location of each detected edge. This could rapidly reduce the delay in the correction of the wheel speed signal during real time processing as the PWE for the particular tooth edge can be logged and stored permanently in the memory. So whenever the vehicle is started, the corresponding PWE for the detected edge can be used for correction without switching on the RLS estimator every time.

The developed processing method is combined with the friction estimation algorithm. However, the resonance frequency estimation from the corrected wheel speeds is still very much dependent on the band pass interval and it is not possible to conclude on the accuracy of the resonance frequency estimate. Hence, more investigation on the estimation of resonance has to be done.

Bibliography

[1] Takaji Umeno. Estimation of tire-road friction by tire rotational vibration model. *R&D Review Toyota CRDL*, 37:53–58, 2002. 1, 2, 6

[2] Danijel Pavković, Joško Deur, Jahan Asgari, and Davor Hrovat. Experimental analysis of potentials for tire friction estimation in low-slip operating mode. Technical report, SAE Technical Paper, 2006. 1, 2, 6

[3] Antoine Schmeitz and Mohsen Alirezaei. Model-based analysis of wheel speed vibrations for road friction classification using mf-swift. In *Proceedings of the 4th International Tyre Colloquium, University of Surrey, Guildford, UK*, pages 20–21, 2014. 1, 2, 6, 58

[4] Fredrik Gustafsson, Markus Drevo, Urban Forssell, Mats Lofgren, Niclas Persson, and Henrik Quicklund. Virtual sensors of tire pressure and road friction. Technical report, SAE Technical Paper, 2001. 1, 6

[5] T Umeno, K Asano, H Ohashi, H Kawai, T Naito, and T Taguchi. Pneumatic monitor for a vehicle based on the disturbance observer. In *Industry Applications Conference, 1996. Thirty-First IAS Annual Meeting, IAS'96., Conference Record of the 1996 IEEE*, volume 3, pages 1687–1691. IEEE, 1996. 1

[6] R.D.Sharma. Developement of an online friction estimator. Technical report, PDEng Report, TU/e and TNO, 2015. 2, 3

[7] Niclas Persson. *Event based sampling with application to spectral estimation.* Citeseer, 2002. 4, 7, 8, 9, 11, 12, 13, 14, 23, 30

[8] Niclas Persson and Fredrik Gustafsson. Event based sampling with application to vibration analysis in pneumatic tires. In *Acoustics, Speech, and Signal Processing, 2001. Proceedings.(ICASSP'01). 2001 IEEE International Conference on*, volume 6, pages 3885–3888. IEEE, 2001. 6, 13

[9] Ralf Schwarz, Oliver Nelles, Peter Scheerer, and Rolf Isermann. Increasing signal accuracy of automotive wheel-speed sensors by online learning. In *American Control Conference, 1997. Proceedings of the 1997*, volume 2, pages 1131–1135. IEEE, 1997. 6, 7, 14, 17

[10] Jacob Svendenius. *Tire modeling and friction estimation*. PhD thesis, Lund University, 2007. 7, 14, 17

[11] Karl Johan Åström and Bo Bernhardsson. Comparison of periodic and event based sampling for first-order stochastic systems. In *Proceedings of the 14th IFAC World congress*, volume 11, pages 301–306. Citeseer, 1999. 12

[12] Rajesh Rajamani. *Vehicle dynamics and control*. Springer Science & Business Media, 2011. 15

[13] Ardalan Vahidi, Anna Stefanopoulou, and Huei Peng. Recursive least squares with forgetting for online estimation of vehicle mass and road grade: theory and experiments. *Vehicle System Dynamics*, 43(1):31–55, 2005. 15

[14] Haykin Simon. Adaptive filter theory. *Prentice Hall*, 2:478–481, 2002. 15, 25

[15] Alan V Oppenheim, Ronald W Schafer, John R Buck, et al. *Discrete-time signal processing*, volume 2. Prentice hall Englewood Cliffs, NJ, 1989. 29

[16] Ronald W Schafer and Lawrence R Rabiner. A digital signal processing approach to interpolation. *Proceedings of the IEEE*, 61(6):692–702, 1973. 30

[17] Fredrik Gustafsson. Rotational speed sensors: Limitations, pre-processing and automotive applications. *Instrumentation & Measurement Magazine, IEEE*, 13(2):16–23, 2010. 30, 32, 34

Appendix A

Robustness of the developed wheel speed signal processing method

Test case 4: Varying wheel speed
The results presented here are evaluated for similar prescribed values as taken in Chapter 5. In this case, a varying wheel speed of $50 + sin(2\pi 0.0125t)$ is considered. Also signal component $s(t) = 0.1sin(2\pi ft)$ with frequency at $f = 45$ Hz is added to the wheel speed signal. The total time for this test case is 80 s. When compared to other test cases, the total time is reduced to 80 s in order to check the robustness of the estimator for lesser number of revolutions of the toothed wheel. The resultant wheel speed and angular distance is shown in Figure A.1(a) and (b) and the wheel speed signal is event based sampled as explained in Chapter 3. The entire results for the wheel speed signal processing is shown in Figure A.2 for this test case.

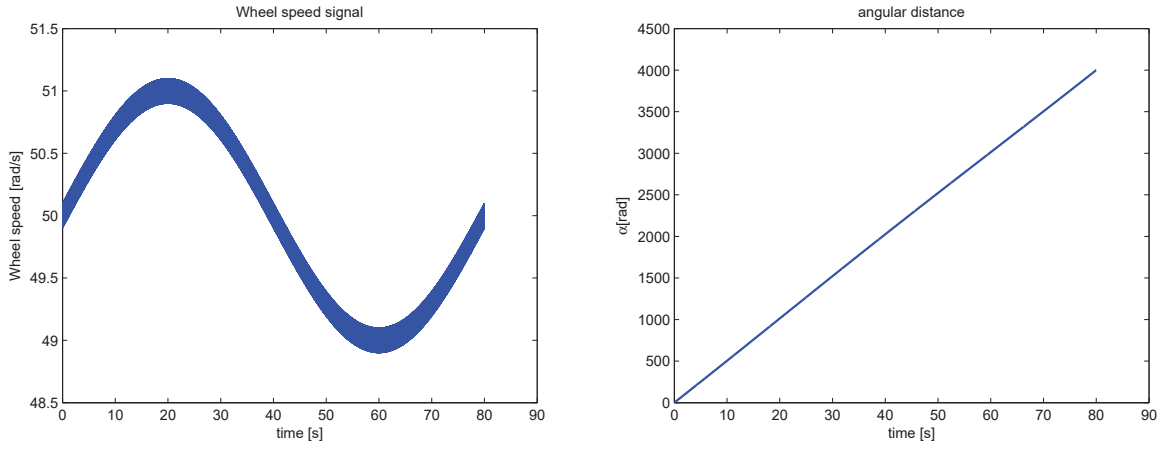

(a) (b)

Figure A.1: (a)Wheel speed signal (b)Angular distance signal

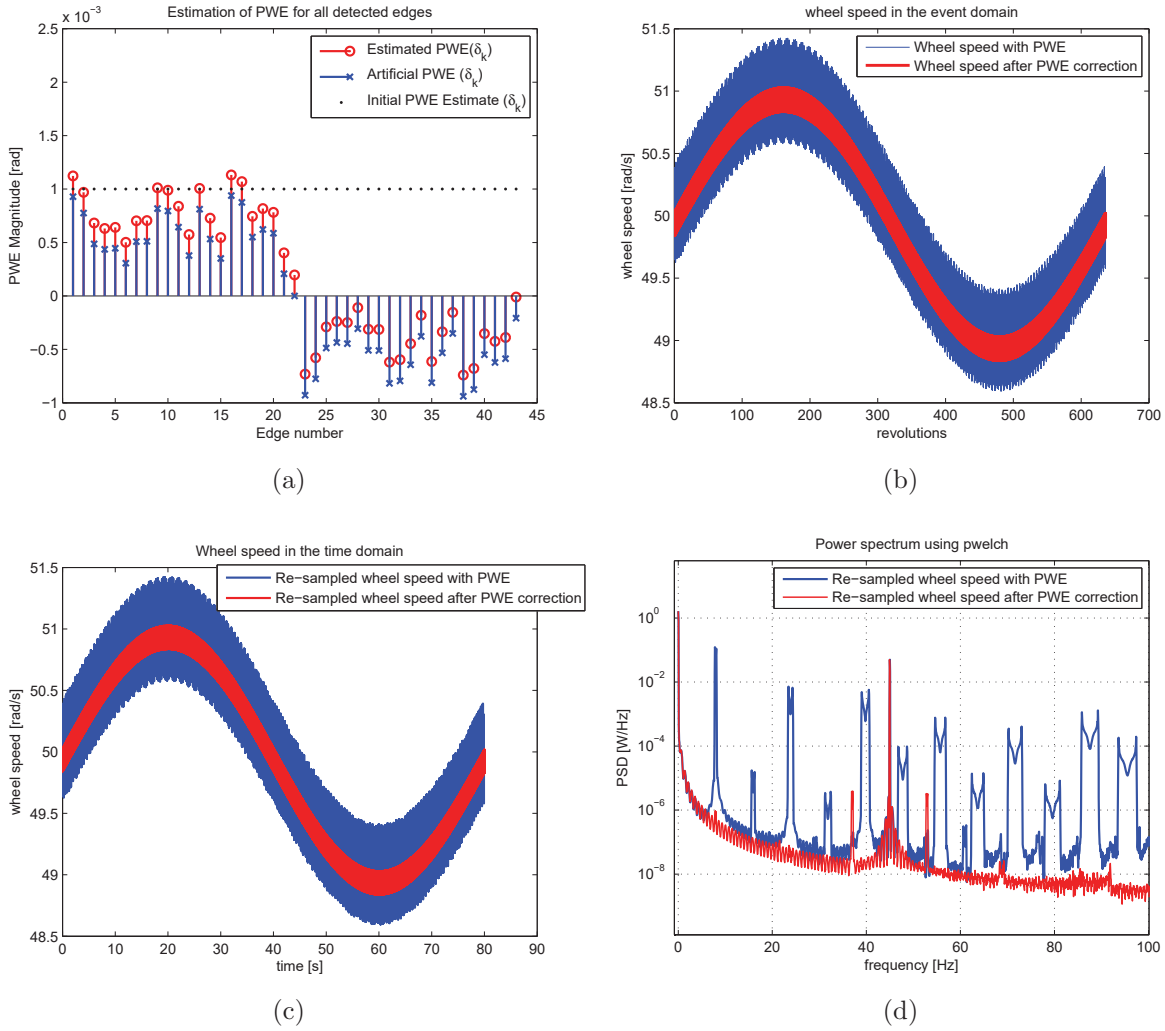

Figure A.2: Wheel speed signal processing results

Event domain phase: The PWE estimate logged at the end of the revolution is shown in Figure A.2(a) and the corrected wheel speed signal after PWE correction is shown in Figure A.2(b). From Figure A.2(a), it can be seen that the PWE estimate logged at the end gives an accuracy of 80% with respect to the prescribed values of the PWE. The accuracy of the estimate is determined by computing the difference between the estimated and the prescribed PWE values. In A.2(b), it can be seen that the influence of PWE is eliminated in the wheel speed signal (as shown in red). Further, the robustness of the estimator with 80% accuracy can be evaluated by checking the wheel speed signal in the time domain.

Time domain phase: In Figure A.2(c), the conversion of the wheel speed signal from the event domain to the time domain is shown. The PSD plot of the wheel speed signal is shown in Figure A.2(d) and it can be seen that the resonance frequency at 45 Hz is visible

in the re-sampled wheel speed signal after PWE correction. The PWE disturbances are attenuated in the re-sampled wheel speed signal after correction. Similar to all 3 test cases explained, the PWE is again clearly seen as harmonics at multiples of the fundamental frequency of the wheel speed signal.

Test case 5: Varying wheel speed

The artificial test case 2 explained in Chapter 5 is again considered in this case. However, the total time is limited to 80 s and the robustness of the developed processing method is evaluated. The wheel speed and angular distance before event based sampling is shown in Figure A.3(a) and (b). The entire results for the wheel speed signal processing is shown in Figure A.4 for this test case.

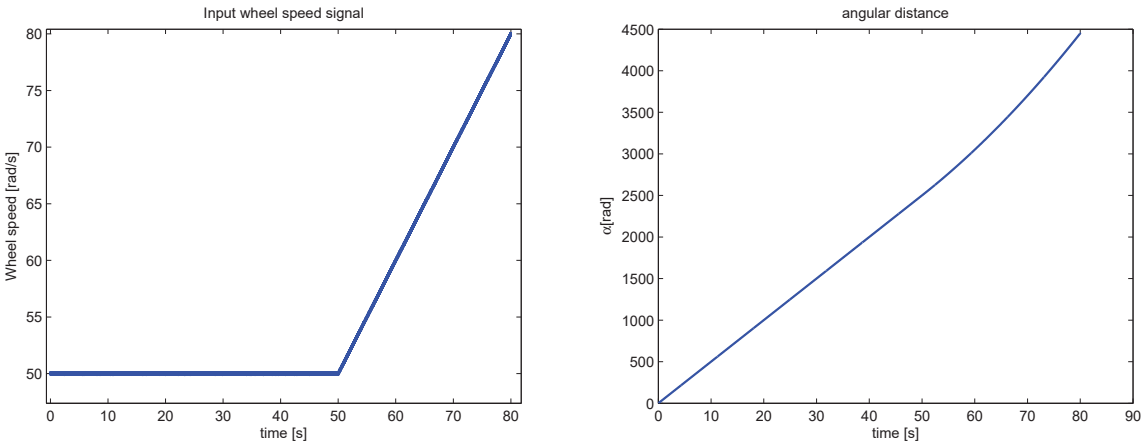

(a) (b)

Figure A.3: (a)Wheel speed signal (b)Angular distance signal

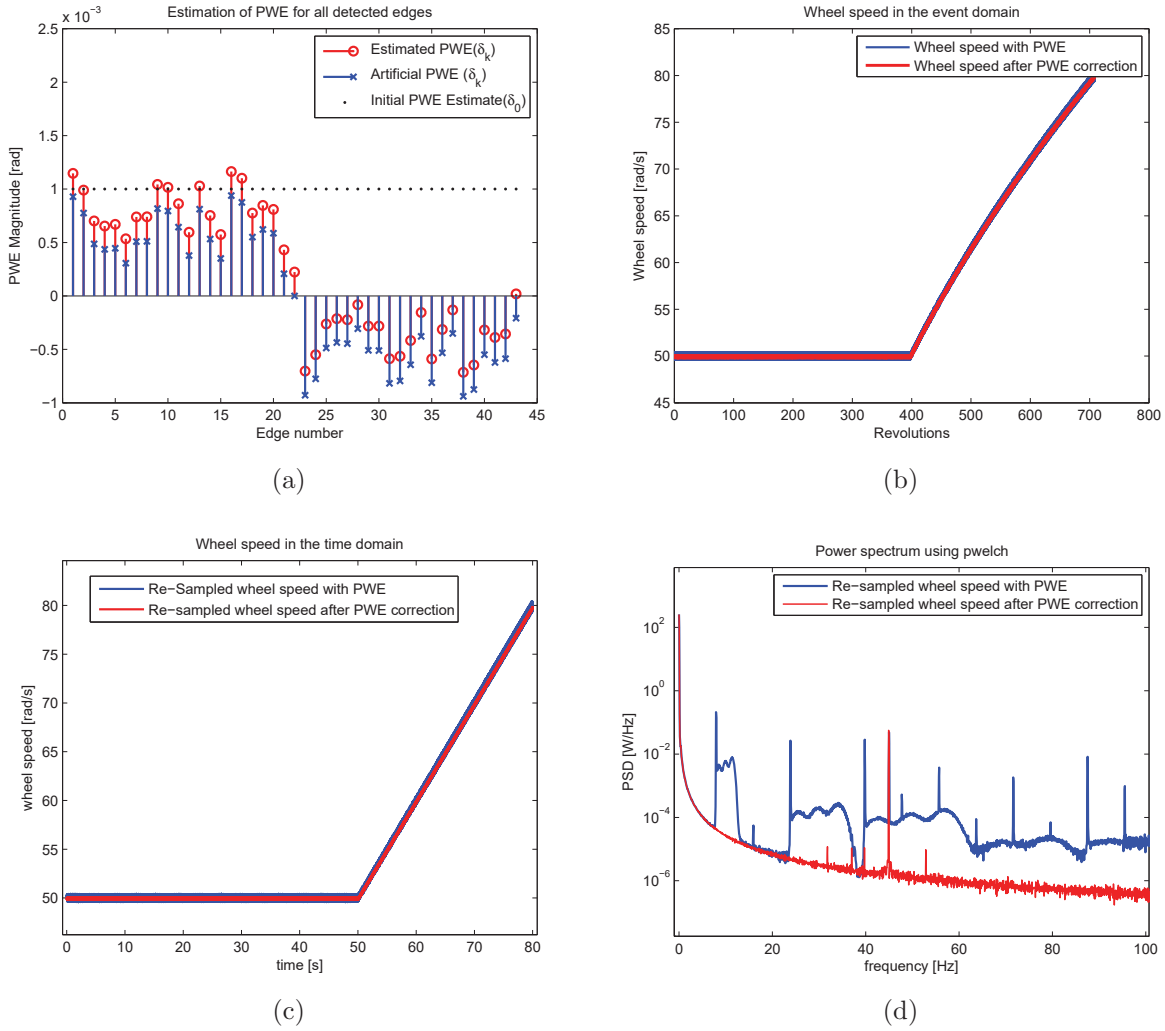

Figure A.4: Wheel speed signal processing results

In this case, the PWE for all detected edges are logged at the end of the simulation and it is shown in Figure A.4(a). The wheel speed signals in the event domain before and after PWE correction is shown in A.4(b) and the re-sampled wheel speed signal is shown in Figure A.4(c). From the PSD plot shown in Figure A.4(d), it can be seen that the PWE disturbance is clearly attenuated in the re-sampled wheel speed signal and a 45 Hz resonance frequency is clearly visible. Hence, from the simulation environment it can be possible to conclude that a 80% accuracy of the PWE estimate is still sufficient to detect the frequency of 45 Hz.